Executive Summary

The information contained in this report involves the testing of labyrinth seals and rating their geometric properties' effectiveness. This project was sponsored by Danfoss-Turbocor in an effort to determine the most effective flow seal at the lowest possible price. The reason labyrinth seals are so vital to their compressors is because they are used in three different "stages" of one of their standard devices. By request of the sponsor air is to be used in place of the typical working fluid R134a.

The test rig uses a design with two pressure chambers that simulate the high and low pressure ratios experienced by a typical Danfoss-Turbocor compressor. The high pressure side of the rig was filled to a maximum of 40 psi where as the low side was left at ambient conditions, any changes in pressure were due to flow through the seal. The low pressure chamber empties into the atmosphere through a converging nozzle. The pressures in both reservoirs were recorded at intervals of 5 psi (based on the high side pressure). Due to time constraints only one seal was tested. The tooth number was manually altered between each test. The tooth of a particular seal was removed in between tests and retested up to 5 total tests. Each tooth count had a concentric and non-concentric test to measure the effect of concentricity on the flow rate. The concentricity was altered using a simple method that relied on gravity to move the plate to a maximum displacement. Micrometer heads were then used to make minute adjustments in either the x or y direction.

The temperatures and pressures recorded at each interval were used in two sets of equations to measure the fluid flow through the seal. The temperature was used to find the fluid properties such as density. The pressures in the two chambers were used in the first set of equations called the "Egli Relations". They were introduced by engineers at Danfoss-Turbocor. The low pressure chamber and atmospheric pressures were used in the second set of equations' involving Mach number relations to determine flow through a nozzle.

The data given by these equations shows that the tooth number plays an important role in the prevention of leakage through the seal. As the seal's teeth were removed, there was an increase in flow through the seal. The results also indicated that decreasing the tooth number had a greater impact on leakage rates at high pressures. The concentricity testing of the different seals showed that it does play a small role in allowing flow to escape.

Table of Contents

1. INTRODUCTION 4

1.1 Problem Definition & Objective 4
1.2 Background Information 4
1.3 Needs Assessment 6
1.4 Product Specifications 6

2. DESIGN SELECTION 9

2.1 Design 1 9
2.2 Final Design 13

3. DETAILED DESIGN ANALYSIS 19

3.1 Flow Measurement Systems & Instrumentation 19
3.2 Shaft Concentricity Adjustment and Measurement 21
3.3 Material Selection 25

4. COST ANALYSIS 26

5. PERTINENT CALCULATIONS 28

5.1 Fluid Properties: Matching the Reynolds # of R134a and Air 28
5.2 Calculations Methodology 29
5.3 Calculation Results 32
5.4 Fluid Calculation Changes 34
5.5 Internal Pressure Vessel Loading 35
5.6 Bearing Load Analysis 35

6. PROOF OF CONCEPT: A PROTOTYPE 38

6.1 Prototype Test Procedure 39
6.2 Prototype Test Results and Analysis 40

7. DESIGN CHANGES 42

8. MANUFACTURING AND FINAL PRODUCT 45

9. TESTING METHODOLOGY 48

10. TEST RESULTS AND ANALYSIS 50

10.1 Relationship between tooth number and mass flow rate 52
10.2 Relationship between concentricity and mass flow rate 54
10.3 Differences between theoretical and actual flow rates 57

11. FUTURE WORK 58

REFERENCES & VENDORS 60

APPENDIX 1: SAMPLE CALCULATIONS 61

Appendix A.1: Egli relations for air 62
Appendix A.1: Egli relations for R134a 65
Appendix A.2: Mass flow rate using Mach number relations 67
Appendix A.3: Propagation of error through the Mach number relations 69
Appendix A.4: Pressure Vessel Analysis Calculations 70
Appendix A.5: Bearing Load Analysis calculations 72
Appendix A.6: Prototype Calculations 74

APPENDIX B: DATA **75**

B.1: RAW DATA ***76***
B.2: MASS FLOW RATE SUMMARIES ***80***
B.3: MASS FLOW RATES THROUGH THE NOZZLE ***83***
B.4: EGLI RELATIONS MASS FLOW RATE ANALYSIS ***87***
B.5 GRAPHICAL RESULTS ***90***

APPENDIX C: DETAIL DESIGN DRAWINGS **94**

1. Introduction

1.1 Problem Definition & Objective

The objective of this project is to design and build a test rig that has the ability to quantitatively determine the amount of leakage across a labyrinth seal. Multiple seal designs of various sizes must be able to be tested. The test rig must also accurately replicate conditions inside a typical Danfoss-Turbocor compressor while using air in place of R134a. Finally a study must be performed using the test rig in order to determine which seal design is the most effective at stopping fluid flow.

1.2 Background Information

According to Flitney and Brown [1], a labyrinth seal operates on following two methodologies: rotating radial faces cause centrifugal separation of liquid or solid from air and a series of restrictions followed by a clear volume creates expansion of a gas and hence reduces the pressure. These seals use a very small gap in between the seal and the rotating shaft, and then grooves are machined into the seal in order to disrupt the flow. A general design of a labyrinth seal is shown in Figure 1 [2]. The fluid is prevented from leaking through the seal by the grooves which induce turbulence and misdirect the flow into the small gaps between each tooth. According to Boyce [2], a labyrinth seal has the following advantages: simplicity, reliability, tolerance to dirt, system adaptability, very low shaft power consumptions, material selection flexibility, minimal effect on rotor dynamics, back diffusion reduction, integration of pressure, lack of pressure limitations, and tolerance to gross thermal variations. Boyce [2] further

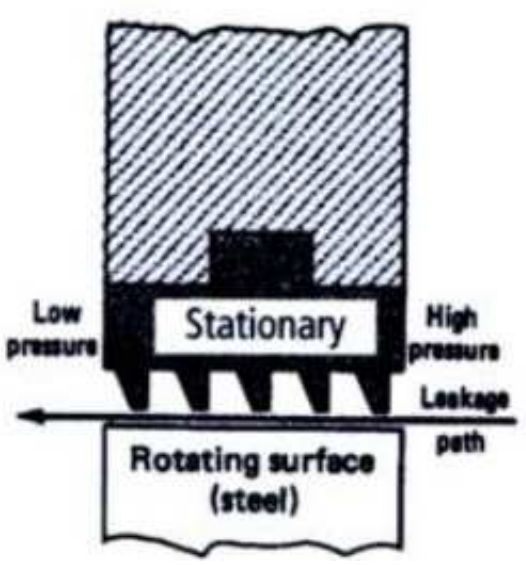

Figure 1: A generic Design of a Traditional Labyrinth Seal

claims disadvantages associated with this type of seal are the following: high leakage, loss of machine efficiency, increased buffering costs, tolerance to ingestion of particulates with resulting damage to other critical items such as bearings, the possibility of the cavity clogging due to low gas velocities or back diffusion, and the inability to provide a simple seal systems that meets OSHA or EPA standards.

There are several variations of the generic seal design (discussed above) currently in use at Danfoss - Turbocor. The designs vary in tooth number, tooth size and spacing, step number, and sizing. Much research has been preformed regarding the labyrinth seal designs, however engineers at Danfoss-Turbocor are uncertain as to what combination of variants will produce the least amount of leakage through the seal.

An experiment was conducted at Texas A&M University in order to determine the most effective configuration of teeth in a labyrinth seal. Figure 2 [3] represents the test rig used in their study. Despite the fact that the Texas A&M study had a more specific focus (tooth size), it will still provide valuable insight as well as numbers to which the results of this study may be compared to.

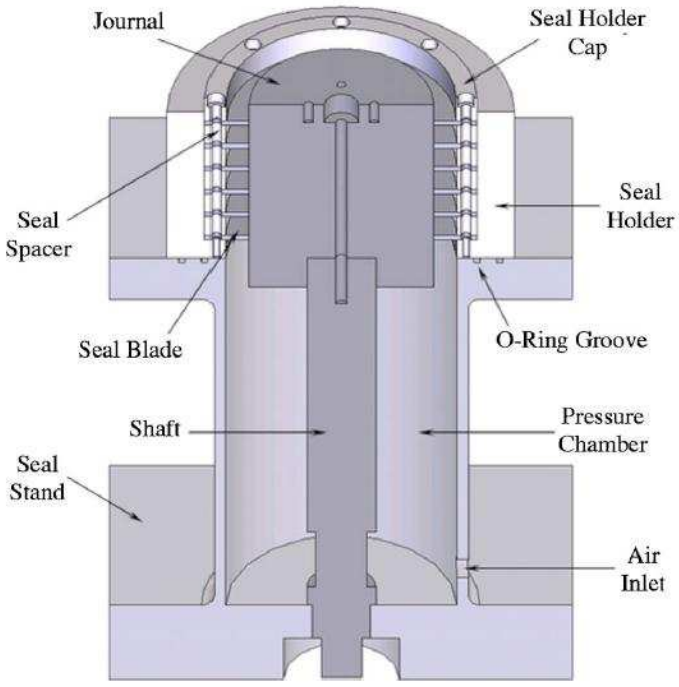

Figure 2: Test Rig used in the Texas A&M University study to determine most effective tooth configuration

1.3 Needs Assessment

Danfoss Turbocor manufactures state of the art compressors for air conditioning systems, and a crucial part of their compressors is a labyrinth seal that prevents the refrigerant from leaking from the high pressure compression stage into the low pressure portion of the compressor. The company has implemented different labyrinth seal designs; however, they have failed to determine conclusively which design yields the most efficient results (I.e. least amount of leakage through the seal). Danfoss Turbocor needs a test rig which will be able to provide quantitative results on the amount of leakage that is encountered at this labyrinth seal. The test rig should be adjustable to fit various seal sizes, shaft alignments, and experience different pressurized testing conditions. It has also been requested that the working fluid of the test rig be air instead of R134A in order to provide a safer test rig and minimize test costs. Danfoss Turbocor also inquired about a possible use of a CFD (Computational Fluid Dynamics) analysis of the seal, but this analysis was revoked from the requirements, due to a lack of experience of this type of software use.

1.4 Product Specifications

In order to make the design process more manageable a coupling matrix was created to match the customer needs with prospective solutions so that product specifications can be created. The coupling matrix shows a connection between what the customer wants and how the design will reflect those needs. The parameters in the horizontal direction indicate what the customer needs where as the vertical direction contains the product specifications. The intersection of the two shows how each specification is relevant to the various needs. The customer has indicated that they need the product to be able to test multiple seal designs, seal sizes, and to vary the shaft-seal concentricity. Simulation of an actual seal conditions inside a Danfoss Turbocor compressor is vital while maintaining relatively low cost. They also would like the rig to be eco-friendly as well as safe to the operator.

Table 1: Coupling Matrix. Listed along the left side are the customer needs, and listed along the top are the product specifications.

		Product Specifications				
		Seal Adapter Plate	Use air instead of R134a	Magnetic Dial Gauge & Micrometer heads	Flowmeter, Pressure Transducers, mass balance system	Pressure Gradient: Shop Air or a Gas Cylinder
Customer Needs	Test Multiple Seal Designs	X		X	X	X
	Test Multiple Seal Sizes	X		X	X	X
	Vary Shaft Concentricity	X		X		
	Eco-Friendly		X			X
	Accurate Internal Compressor Conditions		X		X	X
	Low cost		X			

The "X" indicates where the needs are met

Over the course of designing the test rig several different design options have been considered, but one trait was shared by all options: the need for high and low pressure sides in order to create a differential across the seal. Since pressure is the driving force behind the fluid's movement, it is essential that the test rig incorporate a pressure gradient across the seal in order to accurately recreate compressor conditions.

High Pressure Housing

In order to create leakage, a pressure difference must be created on either side of the provided seal, and to ensure proper calculations of this leakage, the high pressure air being supplied to the system must be held constant. It will be important to know that the high pressure housing does not leak anywhere but the seal itself. This creates the important specification that the

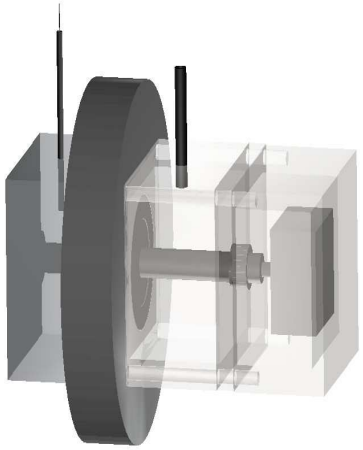

Figure 3: Early Generic Design of the test rig, incorporating a high and low pressure box on either side of the seal.

high pressure housing will have the ability to attach to the seal and provide an airtight connection. Using information provided by Danfoss-Turbocor, the highest pressure seen inside the compressor is near 200psi. It can then be assumed that the high pressure housing of the test rig would not be exposed to pressures higher than those seen at the maximum values of the Danfoss-Turbocor compressor. The design of the test rig should be accompanied by calculations of the forces due to pressure, and should then be able to maintain structural integrity during testing. When considering materials for the high pressure housing, it should be determined which option is most likely to resist deformation and leakage and in order to prevent leakage, the construction of this subsystem should utilize gaskets/o-rings, chemical welding for plastic applications, or standard welding for metal applications.

Low Pressure Housing

This subsystem will not be subjected to the same pressure as the high pressure housing, and therefore will be more flexible in the material selection process. However, this portion of the test rig will be responsible for containing the leaking flow, and therefore it is required that this subsystem be able to eliminate any leakage within the housing.

While there are several other subsystems of the test rig that were involved in making the coupling matrix, Aspects of each subsystem has become more refined than the original broad ideas that were initially used to generate the matrix. As such these ideas will be discussed in detail in later section in this report. These topics include but are not limited to: concentricity adjustments, measurement of flow and concentricity, calculations containing to the Reynolds numbers, and the method used to maintain a pressure gradient.

2. Design Selection

2.1 Design 1

The key component of this concept that differs from others is a high-pressure gas cylinder. From here on the concept will be referred to as “the gas-cylinder concept” for simplicity. For the fluid to flow across the seal, it is dependent upon a pressure difference between the two sides of the seal. In this concept, the high-pressure side of the seal will be maintained by a pressure regulator attached to a fixed-volume high pressure reservoir: a gas cylinder. The gas cylinder will start the experiment with a pressure that is much higher than that required to run the experiment (for example: experiment pressure = 150 psi, cylinder pressure = 2500 psi). The cylinder will contain an initial fixed, measurable mass. The mass of the gas inside the cylinder can be found by making the assumption that the gas inside is an ideal gas, and then by applying the ideal gas law.

$$PV=mRT \tag{1}$$

In equation 1, the variable P is pressure inside the cylinder, V is the fixed, geometric volume of the cylinder, m is the total mass of the gas inside the cylinder, R is a universal gas constant, and T is the absolute temperature of the gas inside the cylinder. The volume of the cylinder is known. By rearranging the equation, the mass of the gas inside the cylinder can be found if the state of the gas is fixed by pressure and temperature simply by rearranging equation 1.

$$m = \frac{PV}{RT} \tag{2}$$

By Applying the Ideal Gas Law before and after the test the mass of air inside the cylinder may be found at both times. Subtracting the final mass from the initial mass in the cylinder will yield a change in mass, Δm:

$$\Delta m = m_{start} - m_{end} \tag{3}$$

Timing the duration of the test the change in mass over time can be found. By definition this would yield the average mass flow rate.

$$m' = \frac{\Delta m}{\Delta t} \tag{4}$$

One problem with this version of the time-averaged calculation is that the test has a start-up time. The start-up time is a result of the development of steady-state conditions inside the high-pressure reservoir on the high-pressure side of the seal, which is located after the gas regulator which is connected to the high-pressure cylinder. This “mid-pressure” zone holds the operating pressure, the high-side pressure, of the labyrinth seal. As an important note: throughout our design we refer to this mid-pressure zone as the high pressure reservoir, but in this document it will be referred to as the mid-pressure zone, or chamber. The mid-pressure is set as a standard operating pressure at which all of the seals will be tested for performance comparisons. During the start of the test, the mid-pressure zone (the high-pressure side of the seal that is maintained/supplied by the regulator and the cylinder) will be at standard atmosphere pressure and will need to be “charged” (pressurized) to the operating pressure. During the charging stage of the experiment, the mass flow rate through the seal is not the same as the steady-state mass flow rate, and will be lower than the steady state flow. The *unsteady flow rate* can be compared across the different types of seals, but this comparison is complicated and beyond the scope of this project.

A more accurate way to find a time-averaged mass flow rate at a standardized pressure would be to wait until a steady-state flow condition has been achieved. At this condition, mass flow rate into the system from the cylinder is equal to the mass flow rate through the labyrinth seal. The related equation is defined as:

$$\frac{dm}{dt} = \frac{PV}{RT} \tag{5}$$

The above equation can be applied twice: it can be applied to the gas cylinder and to the mid-pressure chamber. The volume used in the equation, and for both applications, is constant. The volume is known for the cylinder, but will be difficult to calculate for the mid-pressure chamber due to a complex geometry. Fortunately, the volume the mid-pressure chamber does not need to be known, it is only important that the volume does not change. If volume and the universal gas constant are both constants and do not change with time, then they play an insignificant role in equation 5 (listed below) and the critical parameters become pressure and temperature (which can change with time). If pressure and temperature do not change inside the

mid-pressure chamber, then dm/dt (the change in mass inside the chamber with respect to time) is zero, and the flow state can be considered "steady," hence the term "steady-state condition." For the purposes of this design concept, it is an accurate assumption to treat the mass flow as if it were in steady state.

Graphically plotting the mass inside the cylinder versus time will yield a straight, diagonal line reflecting a constant decrease in mass.

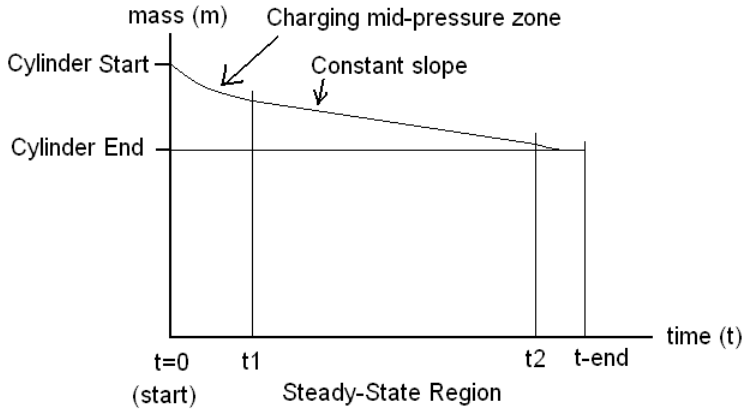

Figure 4: Prediction of the relationship between air mass inside the cylinder and the time over which the test is run

In this graph, t_1 and t_2 correspond to the start and end time across the steady-state condition. The zone corresponding to the constant slope is the steady-state zone where dm/dt in the mid-pressure chamber is zero. Keep in mind that dm/dt is not a measure of the mass flow rate, it is a measure of the mass capacitance in the mid-pressure chamber. As pressure increases and temperature is held constant, the chamber will take in more mass and dm/dt will be a positive value. Below is a graph predicting the mass flow rate through the seal based upon the discussed concept:

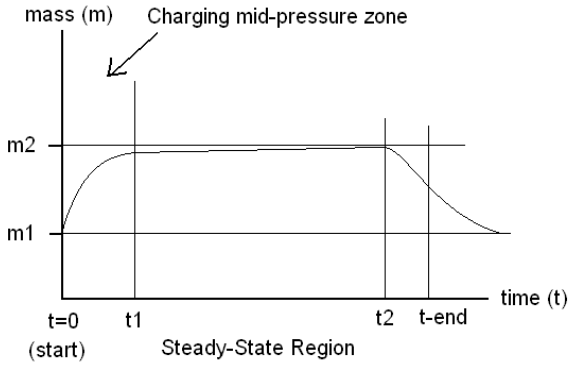

Figure 5: Prediction of mass change inside the "Mid-Pressure" Chamber

In this graph, the slope in the steady state region is shown to be slightly non-constant (exaggerated) to display the asymptotic relation as the experiment attempts to pressurize the chamber while simultaneously leaking through the labyrinth seal. For the purpose of this concept, it would be assumed that the change in mass flow rate during this time period would be negligible, or would be acknowledged and accounted for in error analysis.

Benefits and Drawbacks of the Gas Cylinder Concept

A major benefit of the cylinder method is that it can be used in conjunction with other instantaneous mass flow testing methods such as with a Venturi meter, Orfice meter, or Pitot-probe-utilizing these other methods as a check. If a graph is created that depicts mass flow rate calculated from other methods versus time, numerical integration methods can be used to determine the total mass measured by those meters (The area under the graph would represent the total mass passing through the meter). This total mass can be calculated across a steady-state condition and compared to a result obtained from the gas cylinder.

One of the drawbacks to the gas cylinder method is cost. While the cylinder itself can be rented, the purchase of the compressed air and of the measurement devices is a concern. From one source, Mr. Bill Starch, Machine Shop Manager at the Applied Superconductivity Center associated with Florida State University, rental fees are on the range of 6 to 8 dollars per month, and the cost of purchasing compressed air is close to 6 dollars for a full cylinder. It is not expected that renting to Danfoss Turbocor (DTC)

would cost much more, despite these numbers representing a special FSU-Airgas pricing. The gas cylinder would also require a digital, high-pressure, pressure transducer to monitor the pressure in the gas cylinder, if DTC is unable to provide one, procuring the device could become expensive. This pressure transducer could cost as much as $125, according to Industrial Automation's online store. We would also need a temperature probe, but may be able to work with DTC to avoid having to make a purchase.

2.2 Final Design

The labyrinth seal test rig assembly is comprised of four main subsystems: the high pressure housing, the adjustable seal mount, the low pressure housing, and the structural components. These subsystems work together to perform an analysis of the leakage rates of air through a gap located between the labyrinth seal and the balancing piston. The balancing piston will be rigidly fixed to the shaft, and it will serve as the fixed reference frame for the concentricity adjustments. Each subsystem has components which must operate effectively in order for the entire rig to operate successfully. The following descriptions will explicitly outline how each of these components must be constructed in order to perform in such a manner

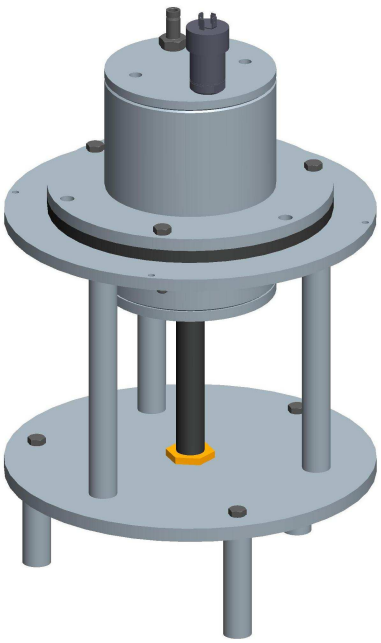

Figure 6: Assembled view of the final test rig design in Pro-E

High Pressure Housing

To properly conduct testing on numerous seals, it is important that each seal be tested under identical conditions. The pressure conditions of a single test must be consistent throughout the entirety of that test, and the conditions should also be consistent over the entire range of tests preformed. To ensure these conditions remain constant, the

high pressure housing must be formed into one solid airtight component. For cost purposes, the ideal method for forming this subsystem into an airtight container will be to weld circular plates onto either side of a cylinder. The following components which are being discussed will be assembled to one another, and form a subsystem which will be referred to as the high pressure housing.

The first component of this subsystem is the high pressure cylinder, and in this application, it will be constructed from a DOM seamless structural round steel tube with an outer diameter of six inches and a wall thickness of one-quarter inch. This item will initially be two feet in length, but will be cut down to meet a specified length. The circular plates which are attached at either end of this cylinder will be machined from a one-half inch thick rectangular piece of A36 steel. These two plates will be referred to as the high pressure cap (upper plate) and the high pressure mount (lower plate). Once the high pressure cap is machined into a circular shape, the only other required machining is a threaded hole which will allow the addition of a quick connect male adapter. The male adapter will allow for an easy connection to the high pressure air source, whether it is a pressure regulator located on a gas cylinder or a connection to shop air.

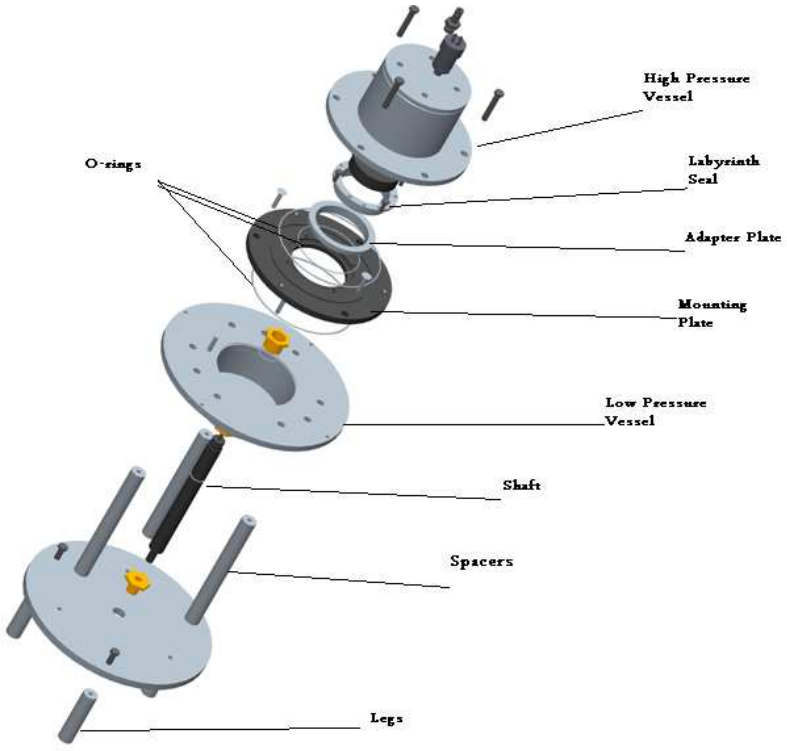

Figure 7: Exploded view of the assembled test rig

This male adapter will have a threaded end which will be configured to install directly into the high pressure cap, and in order to ensure that no leaks are created at this junction, a silicon tape will be wrapped around the threads of the male adapter prior to installation of this component. The high pressure mount will create the connection between the high pressure air source and the labyrinth seal being tested. Therefore, the high pressure mount will be responsible for transferring the pressure force from the high pressure housing to the bolts which secure its position. The high pressure mount will have eight holes drilled through it, and each of these will be offset forty-five degrees from each other at a location four and one-half inches from the center. In order to keep this connection airtight, an o-ring must be in place at the mating surfaces of the high pressure mount and the seal mount.

The high pressure mount, cylinder, and cap will be connected to each other through a two circumferential welds. The American Society of Mechanical Engineers (ASME) has outlined welding standards which should be used for pressure vessels found in the 1998 Pressure Vessel and Boiler Code. The welding geometry that was chosen is depicted in Figure 6a and 6b. (The figures are found in the 1998 Section VIII – Division 1 of the ASME Pressure Vessel and Boiler Codes.)

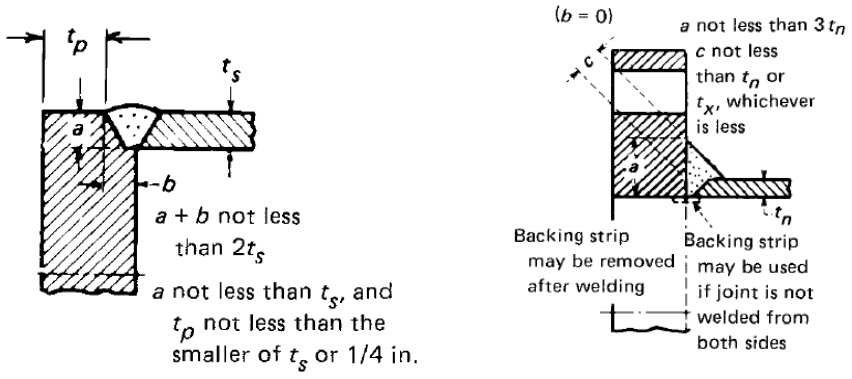

a b

Figures 7a & 7b: Welding geometries for flanged and flat head cylinders

Adjustable Seal Mount

The main purpose of this subsystem is to provide a location for the seal to be connected to both the high pressure housing and the low pressure housing. It also allows

the labyrinth seal to be rigidly connected to a component of the test rig, and also allows the seal to be adjustable relative to the location of the fixed position of the shaft. In order to properly satisfy these requirements, the following important components will be utilized within this subsystem: the seal mount, the labyrinth seal, the differential threading mechanism, and the use of various o-rings.

The seal mount will be machined into a circular plate made from one-half inch thick A36 steel, and it will have eight one-half inch diameter holes drilled through the plate at a radial location of four and one-half inches. These holes will be offset forty-five degrees from each other, and will serve as the standard bolt pattern for each of the connecting subsystems. The labyrinth seal will be mounted directly to the seal mount through the use of four three-eighth inch diameter bolts. These bolts will secure the seal onto to the mount, and they will also create the compression needed to ensure the o-ring is functioning properly. In order to properly use o-rings, a groove must be machined into one of the sealing surfaces. This groove is commonly referred to as a gland, and the sizing of the gland depends on which type of pressure the o-ring will be subjected to, either internal (outward pressure direction) or external (internal pressure direction). The following figure and table was provided by the Parker Hannifin Corporation, and was used as the primary source for determining the proper sizing of the gland:

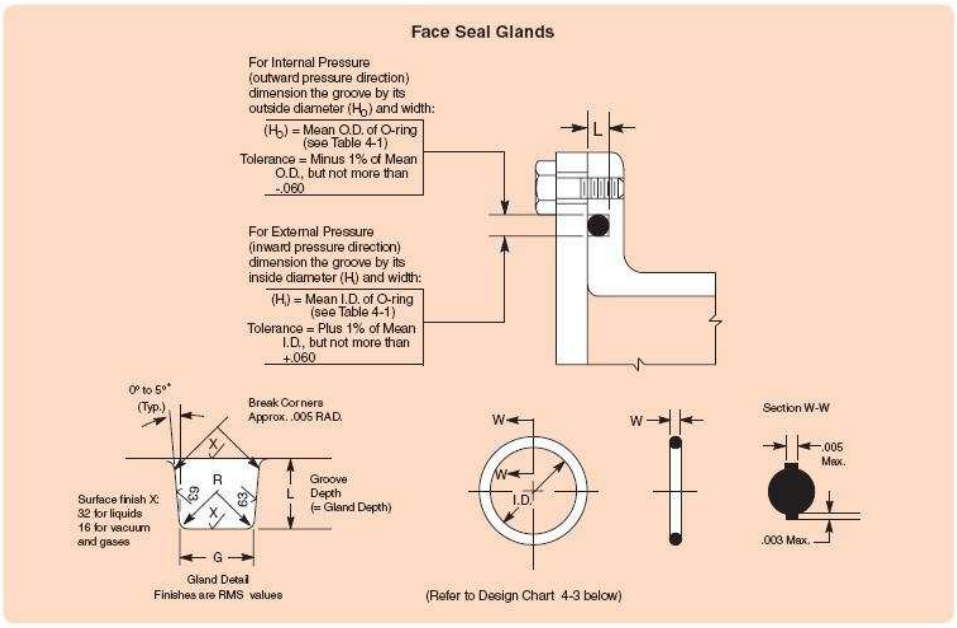

Figure 8: Illustrates location of variables listed in Table 2

Table 2: Used as the primary means to determine the proper sizing of a gland.

O-Ring Face Seal Glands These dimensions are intended primarily for face type O-ring seals and low temperature applications.

O-Ring Size Parker No. 2	W Cross Section Nominal	W Cross Section Actual	L Gland Depth	Squeeze Actual	Squeeze %	G Groove Width Liquids	G Groove Width Vacuum and Gases	R Groove Radius
004 through 050	1/16	.070 ±.003 (1.78 mm)	.050 to .054	.013 to .023	19 to 32	.101 to .107	.084 to .089	.005 to .015
102 through 178	3/32	.103 ±.003 (2.62 mm)	.074 to .080	.020 to .032	20 to 30	.136 to .142	.120 to .125	.005 to .015
201 through 284	1/8	.139 ±.004 (3.53 mm	.101 to .107	.028 to .042	20 to 30	.177 to .187	.158 to .164	.010 to .025
309 through 395	3/16	.210 ±.005 (5.33 mm)	.152 to .162	.043 to .063	21 to 30	.270 to .290	.239 to .244	.020 to .035
425 through 475	1/4	.275 ±.006 (6.99 mm)	.201 to .211	.058 to .080	21 to 29	.342 to .362	.309 to .314	.020 to .035
Special	3/8	.375 ±.007 (9.52 mm)	.276 to .286	.082 to .106	22 to 28	.475 to .485	.419 to .424	.030 to .045
Special	1/2	.500 ±.008 (12.7 mm)	.370 to .380	.112 to .138	22 to 27	.638 to .645	.560 to .565	.030 to .045

The seal mount will have three glands machined into its surface, with two being located on the top surface, and one located on the bottom. The three sealed surfaces will be between the seal mount and the labyrinth seal, the high pressure housing, and the low pressure housing. The sizes of o-rings is governed by the AS 568A standard. The o-ring at the labyrinth seal is an AS 568A standard size 233, and the o-rings at the high pressure housing and the low pressure housing are both the AS 568A standard size 255.

The labyrinth seals used in this test rig will be manufactured by Danfoss Turbocor, and should each have identical bolt patterns, allowing for interchangeability of different seals for a single seal mount. This bolt pattern will consist of four ¼-28 threaded holes, and bolts will used to fasten the seal to the mount.

Differential Threading

Differential threading will be used in order to make concentricity adjustments, however this topic is addressed in the following section: Detailed Design Analysis.

Low pressure housing

The purpose of the low pressure housing is to capture all the air which leaks through the labyrinth seal, and direct this air through a measurable location. The construction of this subsystem will be very similar to that of the high pressure housing, in

that it will consist of the three same major components: a mount, a cylinder, and cap. The low pressure mount and cap have some differences from the high pressure housing, and these will be discussed in detail below. Even though this subsystem will not need to be able to withstand the same pressures as the high pressure housing, it will be constructed with the same procedures.

The low pressure housing has three important functional requirements. It must maintain an airtight connection with the seal mount, it must be supported by the structural components of the rig, and it must channel the collected flow through a measurable location. The mount will be connected directly to the bottom side of the seal mount, and the main purpose for this component is to create an airtight connection between the mount and the low pressure housing. This will be achieved through the use of the o-ring found on the bottom side of the seal mount. The low pressure mount will have the standard hole pattern which align the seal mount and high pressure housing, but four of these holes will have a one inch diameter countersink their bottom surface. These countersinks will allow the mount to be properly positioned on the four structural rods which are responsible for supporting the weight of all the components listed above. The low pressure cap is a critical component in this subsystem. It must provide a location for radial bearings which support the shaft, and it must also provide and outlet for the leaking air to escape. The radial bearing will need to be press fit into the low pressure cap prior to the welding of the low pressure cylinder, as the press fitting of this bearing will be necessary in eliminating any possible air leaks through this location. The cap will have a threaded outlet where an elbow fitting will connect, and this will be responsible for transferring the leaked air from the low pressure housing to the flow meter. The threading of this outlet will require the use of silicon tape to reduce

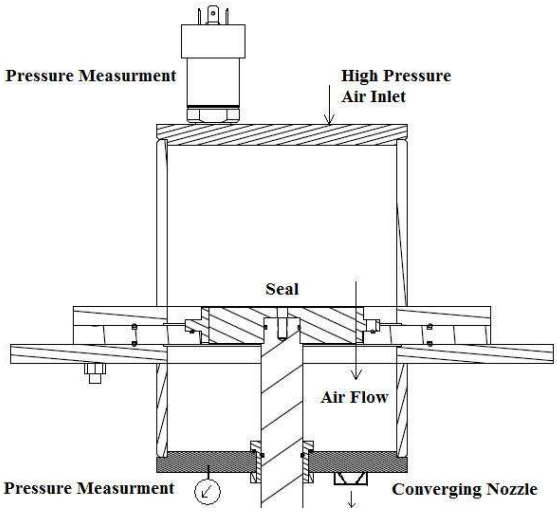

Figure 9: Diagram showing test rig bolted together, air flow, and instrument location.

the possibilities of leakage at this junction. From this elbow, a pipe will extend to the connection of the flow meter.

Structural Subsystem

The purpose of this subsystem is to provide support for each component listed above. This support will be provided by three separate components: the legs, the base plate, and the spacers. The construction of the legs and the spacers will be very similar in nature, as both are one inch diameter steel rods with a threaded hole at either one or both ends. The legs will have one threaded end, which will be rigidly attached to the base plate by the use of 3/8-20 bolts, and the unthreaded end of the four legs will rest freely on the ground. The base plate is a critical component for the support of the rig and also the shaft. The support of the low pressure housing, the seal mount, and the high pressure housing each rely on the structural integrity of this component. The spacers will be rigidly connected to the base plate through the use of 3/8-20 bolts, and each spacer will fit into a one inch diameter countersink located on the base plate. This will aid in the stability of the rig during the assembly, and will allow for an easier connection of the bolts. It is very important to consider the amount of axial loading that will occur due to the pressure force. This load will be distributed through the shaft onto the base plate; therefore the test rig will utilize thrust bearings at this location.

3. Detailed Design Analysis

3.1 Flow Measurement Systems & Instrumentation

A major portion of this project involves the ability to accurately measure the amount of flow that is passing through the seal. In order to ensure the accuracy of the readings found by the rig, there will be three separate methods of measuring the flow so that they may serve as checks against each other. These systems are: a flowmeter, mass balance system for the gas cylinder supplying the air, and finally Pressure transducers which will monitor the conditions inside the high pressure chamber for any pressure drop over time.

The primary and simplest way to measure the flow is using a flow-meter. This will attach to the low pressure chamber of the rig and as the flow moves out to atmospheric pressure it will be recorded. This is the most direct way to measure the flow and it utilizes the advances in technology to measure the flow. A problem that was encountered by using a flow-metering is selecting one in the range estimated for this project. A flow-meters price increases by the range it can measure. For the range that is estimated in this project the flow-meters start at approximately half the allowed budget. Because of the price, it is extremely important that the correct flow meter be purchased. After comparing various meters it was decided that an Omega brand flowmeter model FMA-5000 would be used and will cost approximately $648.00.

The secondary measurement system relies upon a mass balance system for the gas cylinder of compressed air. This concept involves the tank being attached to the high pressure side via hose and a pressure regulator. This regulator will help to maintain the constant pressure gradient by keeping the high pressure side at a steady state. This ensures that a constant velocity will be maintained through the seal due to a constant pressure difference across the seal. This difference in pressure is vital to the leakage through the seal. Changing the velocity by allowing the high pressure side to lose pressure would disrupt the steady state condition. This would make measuring the flow much more difficult and in turn could cause that particular seal to be rated incorrectly.

The tank used for this part of the experiment will be compressed air at an initial pressure of 2500 psi. This large pressure is needed to maintain the pressure of 60 psi (400kPa) inside the high pressure chamber as a nominal value. The time for the experiment to reach steady state is currently unknown, however, the large high pressure air tank will be large enough to last through the trial. These tanks can be rented cheaply, especially with air being the internal gas. The mass of the tank before and after the experiment will be known. This value along with the time over which the experiment is run can be used to solve for a mass flow rate for the leakage across the seal. Assuming no gaps or holes anywhere in the high pressure chamber, the fluid must be presumed to flow through the seal, which can be recorded as the flow rate. The flow rate of each seal should vary and the seal that allows the least amount of flow to pass through will be rated more favorably.

The third check on the system will be performed by Pressure transducers placed inside the high pressure chamber. These will monitor the chamber to ensure that a steady state is maintained and alert the testers should the conditions become otherwise. They will also be able to provide information on how quickly the pressure will drop once the supple is stopped. This information can be used to generate pressure curves over time.

It should also be noted that a pressure regulator and transducer will be used to control and monitory the supplied flow, however, they are not discussed in this section due to the fact that they are used mainly for control and not taking measurements.

3.2 Shaft Concentricity Adjustment and Measurement

Labyrinth seals are a form of non-contact seal. The nature of this seal requires a gap; in this case the diameter of a shaft is smaller than that of the labyrinth seal into which it is inserted. It is theorized that a cylindrical labyrinth seal's performance is based upon, among other factors, the concentricity of the shaft and seal (concentricity is the centering of two circles). Specifically, if the shaft is closer to the seal on one side, it is theorized that the leak rate will increase. The test rig needs to be designed to allow for the measurement of concentricity and also for the alteration of concentricity so that its affect on a seal's performance may be analyzed.

The term 'concentricity' refers to the centering of two circles, one within the other. Concentricity is measured in two dimensions: in polar coordinates, an angle and radius are required. A rectangular coordinate system will take an x and y measurement. Figure 8 shows the two methods of measuring the concentricity of two circles.

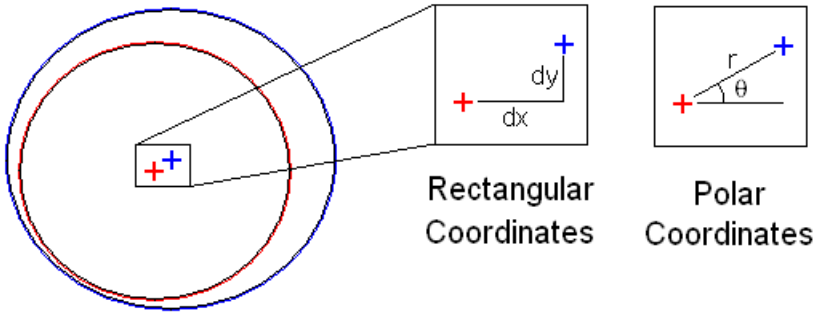

Figure 10: Concentricity measured in both rectangular and polar coordinates

Concentricity Adjustment System

In order to test the effect of concentricity, the capability for adjustment must be designed into the test rig. To do this, either the shaft or the seal must be able to be adjusted and moved in relation to the other. Since the shaft will be fixed to two sets of bearings, it is simpler to adjust the seal position while the shaft remain a stationary reference. In order to facilitate movement, the mounting holes on the seal mounting plate will be larger than the mounting screws protruding from the labyrinth seal design-billet. The labyrinth seal design billet is a cylindrical piece of material with mounting holes in a standardized configuration. The mounting billet will be given to DTC for the machining of a labyrinth seal within specified dimensions. The mounting screws protruding from the labyrinth seal billet will feed through the mounting plate and are tightened with flange washers and nuts to cover the gap from the over-toleranced holes. Designing the holes larger than the screws allows the labyrinth seal a certain amount of freedom, in this case enough freedom to allow for concentricity adjustments.

The shaft and seal concentricity tolerance is on the level of single micron lengths and a movement of that minute magnitude is needed in order meet the needs of the system. The small scale of the tolerance presents a challenge. The devised solution uses a ramp-like system. Essentially, a unit-change in one direction will yield a fractional-change in a perpendicular direction. A highly precise screw-system will be used to accomplish the task of converting the unit changes into fractional moves.

One of the smallest thread pitches, in English units, is the designation 0-80 (zero-eighty), and has 80 threads per inch. A full revolution of this screw gives a displacement of 0.0125 inches, or 317.5 micrometers. Single-degree turns of this screw would yield displacements acceptable for the purposes of this project; however, there are several other factors that must be considered. There is a frictional force between the components that are moving, and calculations predict that with the diameter of a 0-80 screw, an axial deformation on the micron level will be present. In addition to the deformation issue, single-degree turns would be difficult to achieve with human hands. To resolve this problem a smaller thread pitch and larger screw diameter are needed. Unfortunately the next size up had a thread pitch of .355 mm which is too large for the application. To resolve this issue, engineers at Danfoss Turbocor suggested utilizing a ‘differential threaded mechanism.”

The differential threaded mechanism uses two screws of different thread pitches in order to develop a displacement that is equivalent to the difference of the pitches. One of the screws is of a larger diameter and has threads on outer surface as well as a screw hole in the center. This screw is referred to in the mechanism as “the dual-threaded screw,” or DTS for short. The smaller screw, which is inserted into the DTS, has a thread pitch that is slightly different than that of the

DTS. The smaller screw is fixed to the part that will be moved (the labyrinth seal), and the dual-threaded screw screws onto it. The dual-threaded screw also screws into the reference (a flange on the shaft) to which the seal is moving in relation to. Below is a sketch of the differential threaded mechanism. In color, the DTS is green, the smaller screw is blue, the labyrinth seal is pink, and the reference is orange. The small screw and the labyrinth seal are fixed and will not unscrew. In the final design, the labyrinth seal is indirectly attached to the smaller screw. When the DTS is turned counter-clockwise it screws out through the reference and at the same time draws out the smaller screw that is fixed to the labyrinth seal. While the DTS is turning counter-clockwise and screwing out of the reference, the smaller screw is turning clockwise with respect to the DTS. This motion causes the smaller screw to unscrew from the DTS. The result is a displacement of the labyrinth seal about the final reference that is a value of the difference of the two screws' displacements.

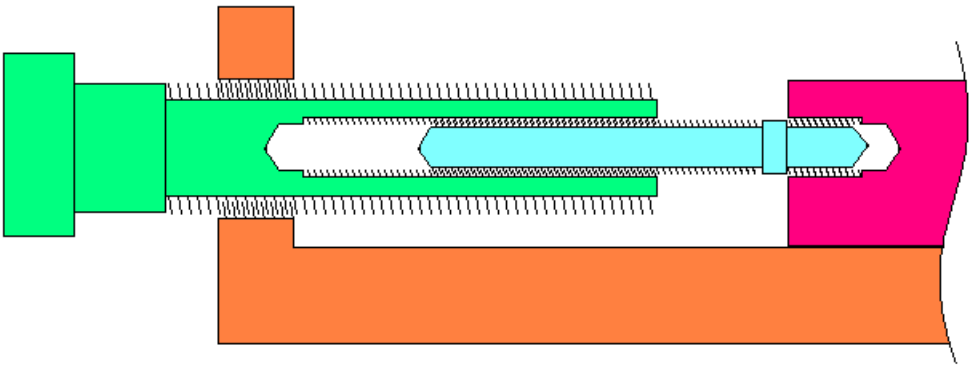

Figure 11: Differential Thread Mechanism Assembly

Dual Thread Dimensions and Assembly

Available resources dictate that the taps and dies used to manufacture the device are in English units. Through iteration and calculations, it has been determined that the mechanism will utilize a larger-diameter screw of thread type 3/8-24 and the smaller screw will be ¼-28. These numbers represent 3/8 inch diameter with 24 threads per inch, and ¼ diameter with 28 threads per inch. The respective thread pitches are 1.058 mm and 0.907mm. For one full revolution, the total displacement is equal to the difference between the two pitches, or 0.151 mm. The total displacement for a turn of 5 degrees would be 2.09 microns.

The multi-threaded system presents unique complications to assembly. The system cannot be assembled with the reference and seal (screw attachment points) pre-fixed. In order to

assemble the system, the mounting bracket must be able to detach from the rest of the system. First, the smaller screw will be permanently attached to the adjustor plate to which the labyrinth seal will be attached. Next, the mounting bracket will be loosely put over the smaller screw (they will not attach due to diameter difference). Next, the dual-threaded screw is screwed onto the smaller screw to a preset distance, thus fixing the mounting bracket in between the labyrinth mount and the DTS. The mounting bracket is then screwed onto the DTS to a preset distance. The entire assembly is then loosely attached to the reference, with the mounting bracket attaching to the reference frame. The labyrinth seal is attached to the assembly. This condition is the "ready position" for labyrinth seal adjustment. Once the concentricity is measured, two of the differential threaded mechanisms will be used to adjust the seal position in an x and y-direction until the concentricity is within a target range. Once the concentricity is verified, under-toleranced bolts (loose diameter) will be tightened to fix the position. This is the ready-to-test condition for concentricity concerns.

Safety Calculations

The stresses in the materials were also calculated. If the contents above the moveable plate weigh 25 lbf, and with a coefficient of static friction for lubricated steel-on-steel of 0.16, the net force to overcome static friction is 17.8 Newtons. This force will generate a deformation in the DTS as well as the smaller screw. With the diameters of the two screws known, the cross-sectional area of the two screws can be found (the DTS has a wall-thickness area). Data was found for the yield strengths and modulus of elasticity for over 20 classes of low-carbon steel. The tensile yield stresses of all of the steels were above 170 MPa, and all of the modulus' of elasticity were close to 180 GPa. Using this information, it was found that the total deformation for a small screw exposed length of 2 cm, and a DTS effective length of 2.5 cm, was 0.124 micrometers. The factor of safety in both parts was over 300, so failure is unlikely for unforeseen loads.

Concentricity Measurement

Due to the minute scale that all of the concentricity adjustments will be made on, it is important that the method used to measure the concentricity be precise. The concentricity will be found by measuring the distance from the shaft's outer diameter to the seal's inner diameter. After reviewing several measurement options, a multi-armed dial gauge micrometer was chosen. Danfoss Turbocor is providing the measuring device from their surplus to ensure that the accuracy needed is met. The gauge is capable of measuring a change in distance between 0 and

1000 microns, which means that if the shaft is off-center by more than 1 centimeter the measuring device will be ineffective. The arms of the gauge are able to be both moved and fixed, with the meter located at the end of the reach. The dial gauge has a strong, magnetic base that can be fixed anywhere so long as the surface is magnetic. The gauge can then take measurements in relation to its position. For instance, If the dial gauge was placed on the stationary rig body and shaft was rotated the gauge would measure any wobble experienced by the shaft.

In the case of this project, the magnetic base will be attached to the shaft, and the arms will position the meter to a cylindrical edge of the seal, perpendicular to the shaft axis. The arms will be fixed in this position. The radius from the center of the magnetic base to the center of the shaft is also fixed. With all of the arms in a locked position, the radius from the center of the shaft to the end of the arm chain is fixed.

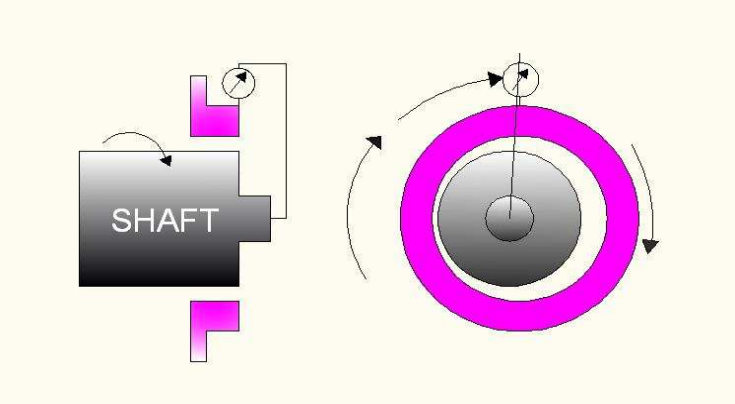

Figure 12: Conceptual diagram of a dial gage. The picture on the left is a side profile while the drawing on the right is from the perspective of looking at the shaft head on

The meter is fixed to the end of the arm chain, and as the shaft is rotated the guage will register any changes in radius in relation to the shaft; I.e. the gauge will measure any changes in the distance from the shaft to the seal. Figure 8 displays a conceptual drawing of how a dial gauge will be utilized in this application.

3.3 Material Selection

After completion of the final design, it was decided to use A36 steel to build the test rig. There were several factors that led to this decision, some of which are: magnetic properties, machine-ability, weld-ability, strength, and price. Although the flow rate through the seal does not depend on any type of magnetic field, the test rig must be made out of a magnetic material in order to accommodate the dial gauge which is to be used for

concentricity measurements. The best way to ensure an air tight seal on the pressure chambers is to weld them closed (accept where the seal attaches). Due to both of these requirements the materials that could be chosen became limited. A36 steel was able to fill both of these requirements. In addition, it is also relatively easy to machine and when bought from an appropriate vendor, fairly inexpensive. In an effort to further decrease material costs a single material was chosen so that a single vendor could be used.

To create the pressure chambers, a 6" diameter, 2' long and ½" thick piece of steel tube will be purchased. A single tube will be purchased in order to save money and it will be cut to length for each pressure chamber. There is some scrap anticipated to be left over from this process. By purchasing a tube, no further machining needs to be done on the tubes other than cutting them to length. Also a cylindrical pressure chamber is able to withstand higher pressures than a rectangular box. Finally, should the need arise for alter the chamber, cylindrical objects can be machined more accurately through use of a lathe over a mill.

In addition to the steel tube, two steel plates and a steel rod will be purchased. The plates of dimensions 2'x 2' x ¼' and 1' x 2' x ½" will be used both to weld shut the pressure chambers. The plates are also ½" thick so that the internal pressure stresses in the chambers are evenly distributed and there are no weak spots that could fail. Finally the steel rod (6ft long) will be cut down and used for legs for the rig body, spacers, and any other miscellaneous parts that may be needed.

4. Cost Analysis

This project was allocated a total budget of $1500.00 dollars to be used for the purpose of purchasing all materials and instruments that are necessary to build and test the labyrinth seal test rig. The budget was essentially allocated to four different areas: raw materials needed to build the rig, pressure equipment needed to test the seals, hardware, such as micrometer heads, bushings, etc, and finally, miscellaneous parts such as o-rings, feet, handles, and knobs. The pie chart bellow shows a breakdown of the budget allocation.

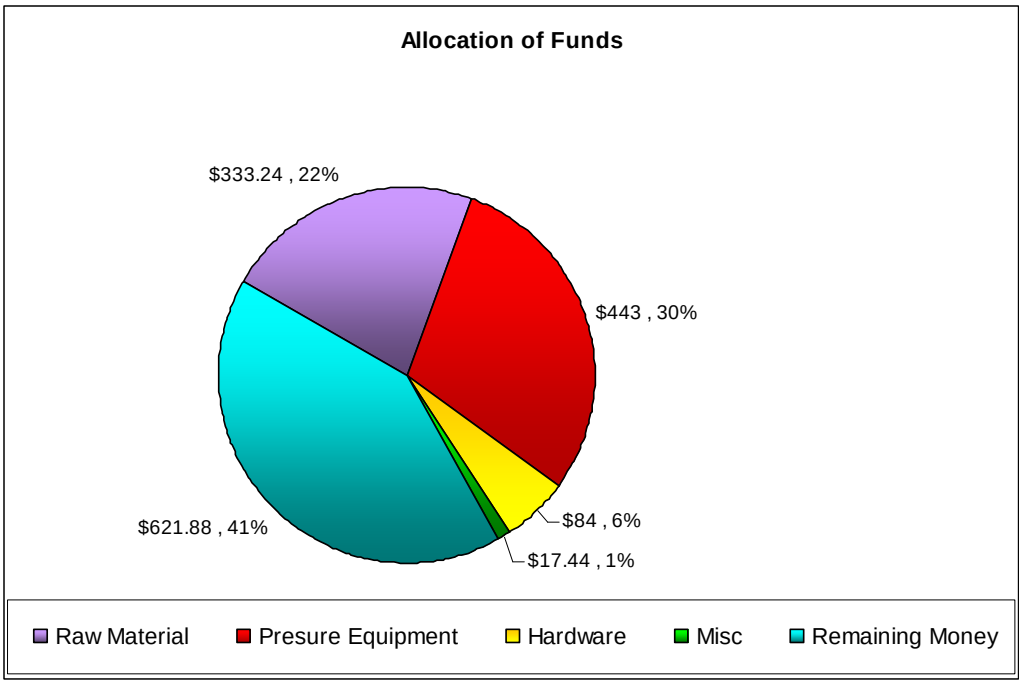

Figure 13: A pie chart showing the percentage of budget and total amount spent on each area

As can be seen approximately 49% of the budget was spent, leaving $621.88 remaining. The largest expenditure was on pressure equipment, 30%, with raw materials being the second largest at 22%. This is in part due to the cost of the materials in each section, as well as the number of items that needed to be purchased. For instance while more o-rings were purchased, they were not nearly as expensive as a single flow meter. An individual cost breakdown is available below in Table 3. A large portion of the budget was able to be saved by Danfoss-Turbocor generously making their spare measurement equipment available for use. They are supplying a dial gauge for concentricity measurements, a pressure regulator for the gas cylinder and pressure transducers for monitoring the conditions in the high pressure chamber.

Table 3: Itemized Cost Breakdown

	Item	Cost	Total Spent	Budget Left
Raw Materials	Steel Tube	$138.14	138.14	1361.86
	Steel Plating	$168.82	306.96	1193.04
	Steel Rod	$25.98	332.94	1167.06
	Threaded Rod	$0.30	333.24	1166.76
Pressure Equipment	Pressure Guage	$16	349.24	1150.76
	Relief Valve	$36.89	386.13	1113.87
	Flow Meter	$201	587.13	912.87
	Pressure Transducer	$125	712.13	787.87
	AC-Dc converter	$49.35	761.48	738.52
	Data Cable	$15	776.48	723.52
Hardware	Brass Bushings	$25	801.48	698.52
	Bushing	$1.24	802.72	697.28
	Tee	$16.52	819.24	680.76
	hex head plug	$1.46	820.7	679.3
	micrometer heads	$39.98	860.68	639.32
Misc.	O-rings	$9.90	870.58	629.42
	Handles	$3.51	874.09	625.91
	Feet	$2.64	876.73	623.27
	Knob	$1.39	878.12	621.88

5. Pertinent Calculations

5.1 Fluid Properties: Matching the Reynolds # of R134a and Air

To be the most use to Danfoss Turbocor the test rig must be able to fit several different designs and sizes of labyrinth seals. For this project three seal designs will be used: Impeller Labyrinths, Main Labyrinths, and Interstage Labyrinths. These three designs represent the various seals that can be found at various locations inside a Turbocor compressor. The figure to the left is a diagram of an impeller Labyrinth seal. As can be see in the diagram there are multiple shaft diameters that vary based on the steps of the seal. For the impeller seals that

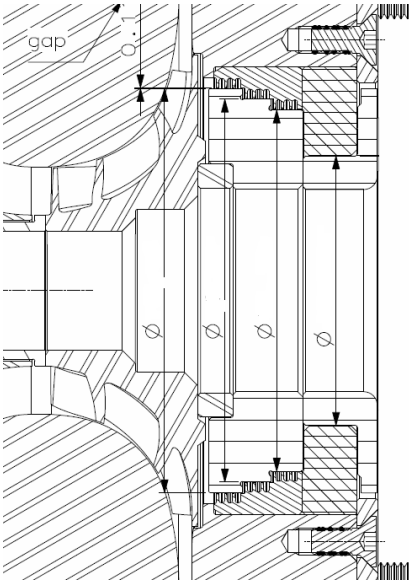

will be tested there are two different sizes which have gap

Figure 14: Diagram of impeller seal. The shaft diameters have been omitted in order to preserve their confidentiality

sizes of 0.8 mm and 0.2 mm. The figure also shows an excellent representation of the teeth on each step which serve a crucial role in the function of the seal. An impeller seal is capable of having 7, 8, or 10 teeth per step. Although not pictured the approximate dimensions for main and interstage seals are also known. The main labyrinth seal design has by far the most possible variations. At its smallest point the shaft diameter is 50 mm through the seal. This is the first of six steps which end in a shaft diameter that is 85.9 mm. The teeth on each step can be varied with the options of 0, 3, 9, or 13 teeth. Also the main seal design comes in several different sizes so that there are several different possible dimensions for the leak gap; they are: 0.091 mm, 0.113 mm, 0.14 mm, and 0.15 mm. Despite the variation in seal diameters, it is, in fact, the dimension of the distance in the gap between the shaft and the seal that carries the most weight. This is the location of the leak and the dimension is the value that will be used to calculate the Reynolds number so that air may accurately be used in place of R134a.

In order to perform accurate analysis on the results yielded by the test rig it is extremely important that a relationship is found between the flow of refrigerant and air. Since the fluid properties of air and refrigerant are extraordinarily different a relationship will be formed based on the calculation of the Reynolds number for each fluid. Part of the problem Danfoss Turbocor is experiencing lies in the fact that certain values, such as the fluid velocity, are unknown at various points inside the compressor. This presented an obvious challenge due to the Reynolds number's reliance on that value. $\mathrm{Re} = \frac{VD}{\nu}$ An alternate methodology to find the Reynolds numbers was needed.

5.2 Calculations Methodology

In 1935 Dr. Egli became the leading authority on labyrinth seals by writing several classical papers which developed working relations that could be used when analyzing flow across the seals. Very little has changed on the topic of labyrinth seals and his relations are applicable to the analysis that needs to be performed for this project. The corner stone of Dr Egli's relations is a formula to find the mass flow rate across a seal with an unspecified number of teeth.

$$\dot{m}_L = \pi d \delta C_t C_c C_r \rho \sqrt{RT} \qquad (6)$$

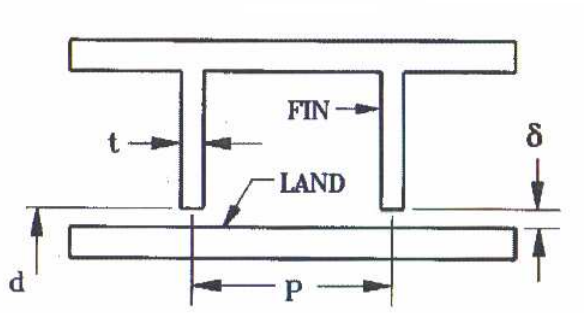

Figure 15: Generic diagram of a labyrinth seal that defines the variables used in Equation 6

The variables referred to in Equation 1 are as follows. "d" refers to the seal diameter, "δ" is the aforementioned gap between the seal and the shaft through which the fluid will be leaking; "t" refers to thickness of each tooth and "p" defines the spacing between individual teeth. Finally the values C_t, C_c, and C_r are all empirically determined values. They are affected by gap distance, number of teeth in a seal, tooth thickness, and tooth spacing. The formulas for these relations as well as the calculations that are outlined and discussed in this section are all available in Appendix A.1. Dr. Egli's relations also call for the fluid properties (ρ- density, R-gas constant, and T-temperature) be taken from the high pressure side of the seal.

Once the mass flow rate was found using Equation 6, the velocity could be determined based on the simple concept of conservation of mass: $\dot{m} = \rho V A$. Using the found velocity, and the gap size for the diameter variable, the Reynolds number could then be calculated. The same process is then performed using the properties of air instead of R134a. The ultimate goal of the calculations is to determine at what operating pressure and temperature the test rig should be run to best match the Reynolds numbers of R134a and air.

While the methodology for calculating and matching the Reynolds numbers appears simple, it is in fact a fairly complex and involved calculation. The complexity appears when the number of possible combinations of diameter, tooth count, and gap size are taken into account. The number of calculations is compounded by analyzing the three possible operating conditions for a Danfoss Turbocor compressor. Conditions 1 and 2 are

both common conditions and they correspond to water cooled and air cooled applications respectively. Condition 3 is an extreme condition where the compressor experiences a high pressure ratio, however, this is a rare condition.

Table 4: Summarizes the pressures and temperatures that can be seen in a typical Danfoss Compressor at 3 different operating conditions

	Condition 1	Condition 2	Condition 3
Saturated Suction Temp (degC)	5.5	0	-2
Saturated Discharge Temp (degC)	36.1	50	55
Ps_{uct} (Kpa)	255	192	171
P_{disch} (Kpa)	813	1217	1391
P ratio	2.57	4.50	5.49
ΔP (Kpa)	558	1025	1220
Pi	469	520	536

ΔP main labyrinth	558	1025	1220
ΔP 2nd impeller labyrinth	255	192	171
ΔP1st impeller labyrinth	303	833	1049

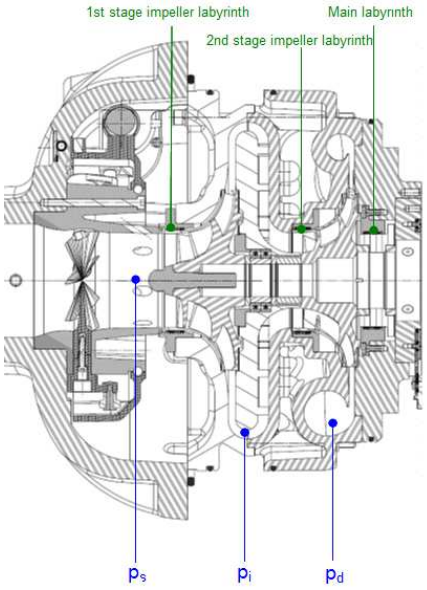

Figure 16: Accompanies Table 4 in displaying location of values

5.3 Calculation Results

When performing the necessary calculations to match the Reynolds numbers several factors needed to be taken into account for determining the test rig run conditions. The first is that the air in the high pressure chamber is at atmospheric (or room) temperature. This was done in order to eliminate designing or purchasing a heat exchanger to heat or cool the air to a specified temperature. By doing so the design was able to be made simpler and the budget was able to be conserved. The client also agreed to the temperature restriction. It is also important to take into account the pressure at which the high pressure chamber will be pressurized to due to equipment constraints. For instance, the Reynolds numbers may be able to be matched exactly at 500 MPa (This is an arbitrary number used for illustration), however, the ability to supply that high of pressure from a gas cylinder is unlikely. For this reason, pressures above 1 MPa were not considered in the calculations. Ultimately, it was decided that the best possible operating pressure for the test rig was 400 kPa (58psi). This choice was influenced by a relationship between mass flow and pressure that was discovered while testing the design prototype. This relationship is discussed in greater detail in the section devoted to the prototype.

The interstage labyrinth seal is the smallest of all the seals and also has the least variation in design combinations; these qualities make it an appropriate place to start the analysis of calculation results. The mass flow rates that are listed below are the mass flow rates of air at 400 kPa. The largest mass flow rate that was seen across a seal was 0.023kg/s and it occurred at the seal diameter of 25.64 mm, a gap size of 0.18mm and 10 teeth. The lowest accurately calculated flow rate is .015 and occurs at a seal diameter of 29.64 mm with 7 teeth (there is only 1 possible gap dimension). The qualifier “accurately” is used due to a problem that was encountered when attempting to perform the calculations for 3 teeth. The empirical formulas that are used in the calculations require constants to subtracted from the tooth number (or some variation on the tooth number I.e. ln) which in this were larger than 3 (tooth number). The result of this is that the equations yield a negative number for the mass flow rate and the Reynolds number. While no numerical values can be found for this circumstance it can be inferred that there is a minimum number of required teeth for the interstage seal design, which is in this case 4. This information may play an important role in later analysis of the seal performance.

The impeller seal design is larger and had more possible combinations: there are 4 possible diameter, 2 different gap sizes, and 3 different tooth counts. The largest and smallest mass flow rates were: 0.051 kg/s and 0.031 kg/s. The largest flow rate occurs at a seal diameter of 89.2 mm, a gap of 0.18mm, and 8 teeth. Meanwhile the smallest mass flow rate occurs at 2 separate seal diameters, 66mm and 67mm, at a gap of 0.18mm and 7 teeth.

The Main seal calculations were the most intensive due to the fact that there were 6 possible diameters, 4 gap sizes, and 4 different teeth counts. A variation on the previous calculations was for this seal design due to possibility of 0 teeth. One of the empirical formulas (please see Appendix A.1) requires taking the natural log of the tooth count. Since doing so for 0 teeth would yield impossibility, it was assumed that the variable relying upon that particular formula (C_t) was equal to 1. The normal method was used for calculating the mass flow for all other cases. The largest mass flow rate occurred at a seal diameter of 85.9 mm with a gap dimension of 0.15mm and 0 teeth with a value of 0.225 kg/s. Because that value is found using the special condition it is excluded and the next largest flow rate was 0.049kg/s and was located at a seal diameter of 85.9mm, gap dimension of 0.15mm and 9 teeth. The lowest flow rate was 0.011 kg/s located at a seal of 50 mm diameter, gap size of 0.15 mm and 3 teeth.

Although specific numbers are not mentioned in the body of this report, the calculated Reynolds numbers of air and R134a are not on the same order of magnitude and therefore do not match. After analysis of the results it was determined that matching the Reynolds numbers without altering the input temperature would be extremely difficult. Since the Reynolds number of R134a was several orders of magnitude larger than that of air (in most cases), scaling up the test rig was considered as a possible option to increase the Reynolds number of air. Unfortunately since most of the dimensions are on a micron level, the scale of the rig would need to be increased many times before any significant effect would be felt by the Reynolds number. Scaling the rig that amount would make it infeasible to build or keep for later use by Danfoss Turbocor. For these reasons it was determined to keep the rig at the original dimensions. Instead of matching the Reynolds number to determine at which pressure and temperature the rig should run at, the test rig will be subjected to a pressure of 400kPa and atmospheric temperature.

The relations previously calculated will then be used to perform a numerical analysis on the seal performance and compare the actual results to the theoretically projected results. It is believed that so long as each seal is tested under the same conditions the results will still be valid so long as an accurate numerical analysis is performed.

5.4 Fluid Calculation Changes

As the design process progressed into the spring semester, Danfoss Turbocor was able to present a refined list of seals that they would be providing for testing. The list included an impeller seal, two interstage seals, and one touchdown bearing seal. Also, an error in the provided analysis conditions was found. The combination of these two events lead to the previous calculations being redone, using new pressure ratios. The calculation methodology was not changed and Egli's relations were still used. The major change was that the calculations were able to be compacted since individual seal specifications were available, which removed the need to perform calculations at all possible diameters, tooth counts, etc. A sample calculation of the Egli method is available in Appendix A.1, and the table below summarizes the theoretical flow rates for each seal for both air and R134a. The calculations for the mass flow of R134a were performed at both compressor conditions (temperature equal to 36^{o}C and a pressure ratio of 0.88) as well as the test conditions (temperature of 24^{o}C and a pressure ratio of .244) in order to provide the most accurate comparison.

Table 5: Summary of theoretical mass flow rates through specified seal types for both air and R134a.

Seal Type	Seal diameter (mm)	R134a mass flow Compressor Conditions	R134a mass flow (kg/s) Test Conditions	Air mass flow (kg/s)
1st Stage Shrouded Impeller	93	0.169	0.157	0.06
Interstage W 15.48	33.6	0.06	0.055	0.021
Impeller S1.70	89.65	0.1385	0.126	0.048
Touchdown Bearing and Seal	75	0.029	0.027	0.01

5.5 Internal Pressure Vessel Loading

It was determined that for safety reasons the forces experienced by the pressure inside each pressure chamber should be analyzed so as not to exceed the test rigs capabilities. Each chamber is made out of A36 steel, .635cm (½") thick tubes and 0.14 m (5.5") in diameter. A36 Steel has a tensile strength of 180MPa. With the pressures of the high and low sides known, 400kPa and 101kPa, it becomes a very simple matter to analyze the hoop and longitudinal stresses.

$$\sigma_1 = \frac{\mathrm{Pr}}{t} \tag{7}$$

$$\sigma_2 = \frac{\mathrm{Pr}}{2t} \tag{8}$$

Equations 7 and 8 show the formulas used to find the hoop and longitudinal stresses respectively. Based on these values, the high pressure chamber will experience a hoop stress of 5.51MPa and a longitudinal stress of 2.76MPa. The low pressure side will experience a hoop stress of 2.22 MPa and a longitudinal stress of 1.11MPa.

The factors of safety are found by dividing the tensile strength by the hoop or longitudinal stresses.

$$FS = \frac{\tau}{\sigma} \tag{9}$$

Based on this formula the high pressure chamber has a factor of safety of 32.6 and 65.3 in the hoop and longitudinal directions. The low pressure side also has very high factors, 80.8 (hoop) and 161.5 (longitudinal). Based on these calculations it is determined that the test rig will be able to withstand all foreseen testing conditions. Complete calculations of the stresses and factors of safety can be seen in Appendix A.4.

5.6 Bearing Load Analysis

While testing of the rig will be done without the rotation of the shaft, the client would like the option for rotation to be included in the design should they choose to add a motor at a later date. Rotation of the shaft will require the support of two bearings in order to withstand the forces generated. The bearings will be located towards the bottom of the test rig; one located on the outside and one inside the low pressure chamber. The

bearing furthest from the seal will serve as the thrust bearing while the other will be the radial bearing. Ball bearings were selected for this application. Due to the possibility of very high speed rotations (approximately 10,000 RPMs) ball bearings were selected over roller bearings as they are better suited for high speed applications.

The process for selecting a bearing is a lengthy one. The first factor needed for the bearing information is the fatigue life. The projected lifetime of the bearings is solved for in millions of revolutions by multiplying time by the rotational speed. The time was estimated to be 10 hours. The projected lifetime is only a reference value. However, the bearings themselves will run for much longer than the 6 million revolutions predicted. This factor is to account for any possible fatigue loading the bearings will endure.

The loads on the bearings were the next factors that needed to be calculated. This was done by finding out the surface area exposed to the high pressure side of the rig. The maximum pressure reached inside the rig is estimated to be 100 pounds per square inch (400 kPa). Once known, the area was multiplied by this maximum projected pressure inside the rig to find the force acting in the axial direction. This value was found to be around 5.6 kilo Newtons. Since the test rig is set up in a vertical arrangement, the weight of the shaft is also supported by the bearings. This weight was added to the force of the pressure to find a total axial pressure, however, the weight of the shaft was insignificant in comparison to the force caused by the pressure chamber. The bearing must meet this force requirement in order for the rig to maintain stability. The radial force has a negligible effect on the total force exerted on the bearings due to the rig's vertical orientation. A radial force was arbitrarily chosen to be a non-zero value of 90 Newtons.

The total force exerted can be used to solve for the dynamic load factor 'C', which is one of the two dominant force factors in bearing selection. The other factor to consider is the static load, 'C_0', which represents the amount of load that the bearing supports with no rotation of the rings before dimpling on the bearings will occur. Once the static and dynamic loads have been determined, a bearing must be chosen with a dynamic load close to the value given by the total force and projected lifetime. The dynamic load was calculated to be 18.775 kilo Newtons. The bearing chosen was 63/22, which has a dynamic load of 18.6 kilo Newtons.

An iterative process was used to determine whether or not the bearings would meet the indicated requirements. Before the equation for equivalent load can be applied, several unknown factors must be determined. The unknowns include the rotation, thrust, radial factors and the radial and axial loads. The rotation factor was found to be 1 because the inner ring, not the outer ring, of the bearing rotates. The radial and axial loads are the values that were previously calculated. To solve the radial and thrust factors the axial load must be divided by the static load. The value given by the division of these two numbers yields a reference value "e" from the SKF bearing reference tables from the referenced text (Machine Design: an Integrated Approach). The ratio of axial to static load was found to have a value of .602. An interpolation can then be performed to find the value of "e" corresponding to the correct location in the table. Once "e" is known, it can be compared to the ratio of the axial force to the radial force. Depending on the comparison a different set of radial and thrust factors may be needed. In this application the thrust force is much greater than the radial force so the ratio of forces is larger. The column used gives a value of .56 for the radial factor and roughly 1 for the thrust factor. With all values in the equivalent equation solved for the load was found to be 5.6 kN. This load was used in the dynamic force load equation incorporating projected lifetime and the end result was 18.9 kN.

The final calculated dynamic load is .116 kN, which is more than the original dynamic load of the selected bearing. There is a 0.6% difference in the two values making the selected bearing appropriate for this application.

Another important aspect of this bearing selection is the diameter of the inner ring. The bearings chosen has an inside diameter of 22mm which is smaller than the shafts diameter of 25.4mm. This will require machining of the shaft in order to accommodate the bearings. As the diameter of the bearings increase the load they can withstand increases as well, however, the rotation they can be subjected too decreases. As stated before, this application requires a maximum speed of ten thousand revolutions. The decision was made that acquiring the correct load and allowing it to safely rotate at the maximum anticipated speed took precedent to the inner ring diameter. The shaft can be easily machined to comfortably fit the bearings in place. It must also be realized that the dynamic load calculated for the bearings is not the load the bearings will endure.

This is merely a safeguard for the bearings incorporating the life cycle of the bearings and the rotation that they will subjected to. The calculations that correspond to the method described in this section are available in Appendix A.5

6. Proof of Concept: A Prototype

After the final design had been decided upon, there were several concerns on whether the theory would actually work. In an effort to confirm the hypothesized behavior a prototype of the test rig was built out of wood using the scrap parts (seals) that had been provided by Danfoss Turbocor. Specifically, it was hoped that the prototype would confirm methodology of finding the mass flow rate. By verifying the mass flow calculations, an accurate approximation of the flow rate of air through the test rig could be made. Using this information a flowmeter could be decided upon. Due to the precision and cost that is typically associated with flow meters it was important to know the range over which it would be taking reading in order to avoid purchasing a meter that would prove ineffective. Confirmation of the mass flow rates would also provide insight into the feasibility of measuring the pressure drop over time in the high pressure chamber. There were concerns that the leak might be great enough to prevent steady state pressurization from being achieved in the chamber before the seal. It is important that the air leaves the chamber slow enough to pressurize the chamber as well as allow the pressure to drop in a measurable period of time.

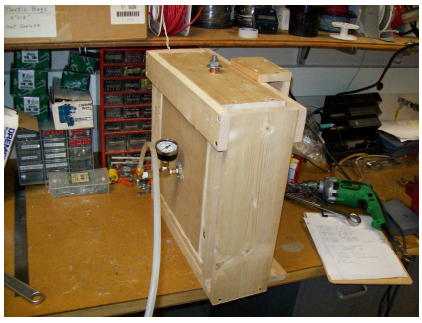

Figure17

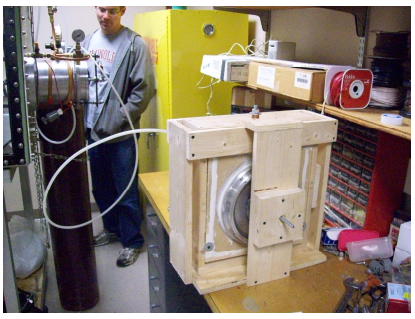

Figure 18

Figure 17 & 18: Shows the front and back of the prototype.

The prototype measured the mass flow across the seal by measuring the mass change inside the gas cylinder. Also Nitrogen was used in place of air due to the

availability of nitrogen cylinders. The test was conducted at several pressure differentials, with the low pressure being ambient air pressure. During the prototype testing, several dynamic side effects were noticed. First, the gas cylinder became very cold. The temperature of the gas inside the cylinder is hypothesized to decrease with decompression, and to reach an equilibrium value where the temperature of the air in the cylinder is constant (do to non-adiabatic conditions of the cylinder). The point at which a hypothetical temperature equilibrium is reached is still under investigation. The second occurrence noticed pertains to pressurizing the high-pressure side of the labyrinth seal. The flow was increased from zero to a certain unknown value, m_0, before the pressure inside began to increase above atmosphere pressure. After m_0 was attained, a small increase in supply produced an immediate increase in pressure. This seemed to indicate that there is a "bottle-neck," or limiting factor to the flow. Analysis of test data from the final design tests is expected to show a correlation. The last, and perhaps the most important, is the required mass change in the cylinder to obtain statistically-relevant, time-averaged analysis of the mass flow: four tests with the prototype used a total of 64% of the total mass in the cylinder. Note that there is a mass loss during non-steady-state stabilization.

6.1 Prototype Test Procedure

Before beginning the test, a check to insure all of the necessary components were attached to the test rig was performed. The pressure was then turned on and the fluid began to flow into the high-pressure chamber. Flow was increased until the high-pressure chambers' pressure gauge began to indicate an increased pressure. The flow was then carefully adjusted to the operating pressure (this adjustment is small compared to initiating the flow to read a pressure increase). Steady-state conditions inside the high-pressure chamber are created as quickly as one can adjust the pressure regulator on the gas cylinder (with exception of temperature).

Once the operating pressure was reached data acquisition could begin. For the prototype, this included writing down simultaneously the time and pressure inside the high-pressure cylinder. The pressure graduations on the cylinder were in kilogram-force per square centimeter (kgf/cm^2), and one kilogram-force is equal to 9.80665 Newtons.

The graduations on the gauge were every 5 kgf/cm^2. The pressure gauge on the high-pressure chamber had graduations at every 1 psi. The high-pressure chamber pressure gauge starts at 1 psi, so it is assumed that the gauge is not accurate at or below 1 psi. The tests were conducted across a change of 15 kgf/ cm^2, according to the high-pressure cylinders' pressure gauge. Sample calculations of the work performed to determine the time averaged mass flow rate (during steady-state conditions) is available in Appendix A.6

6.2 Prototype Test Results and Analysis

Below are the technical results from the prototype test.

Prototype Supply Gas Cylinder US DOT Designation: 3AA2400
Standard Internal Volume: 49.9 Liters

Table 3: results of tests performed on the wooden prototype

	Test 1	Test 2	Test 3	Test 4
Steady-State Pressure	2 psi	3 psi	4 psi	5 psi
Temperature (est.)	0° C	0° C	0° C	0° C
Cylinder Gas Mass Start	7.133 kg	5.992 kg	4.851 kg	3.424 kg
Cylinder Gas Mass End	6.277 kg	5.136 kg	3.995 kg	2.568 kg
Cylinder Gas Mass Change	0.856 kg	0.856 kg	0.856 kg	0.856 kg
Elapsed Test Time	140 s	185 s	110 s	147 s
Measured Mass Flow	0.00611 kg/s	0.00463 kg/s	0.00778 kg/s	0.00582 kg/s
Predicted Mass Flow	0.003625 kg/s	0.004202 kg/s	0.004635 kg/s	0.004976 kg/s
Measured Volumetric Flow	311.469 L/min	235.706 L/min	396.415 L/min	296.637 L/min
Predicted Volumetric Flow	183.712 L/min	212.946 L/min	234.891 L/min	252.139 L/min

Overall the prototype was very successful in achieving its intended purpose. Upon looking at the data several concepts were able to be confirmed. Perhaps the most substantial, is the accuracy of the mass flow equations in predicting the flow rate through the seal. This allows a flowmeter to be chosen with a high degree of confidence in the selection's ability to perform under the conditions that the test will be conducted under. Also it was proven that the high pressure chamber can be pressurized and reach a steady state before starting data acquisition.

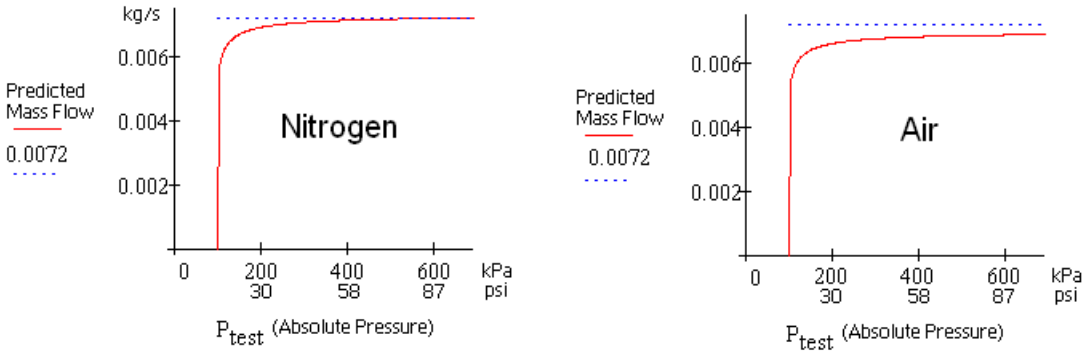

Figure 19: Graphs of the mass flow rate vs pressure for Nitrogen and Air

The above graphs illustrate two very important concepts. There is a minimum flow rate needed to generate a pressure gradient and there is also a maximum flow rate that can be achieved; once this flow rate is achieved it will not increase despite increases in pressure. Based on the results found during this test, the minimum required flow rate is approximately 0.005 kg/s. The mass flow rate also appears to asymptote at approximately 400 kPa (approximately 58 psi). It is partially due to these results that the decision to run the actual test rig at 400 kPa was made.

Error sources in the measured numbers come from unmeasured temperature changes, pressure gauge accuracy, misalignment of the shaft and seal, and a single knot in one of the planks in the wood that allowed a small leak. An exact error analysis was not performed due to the knot leak generating an unknown error.

7. Design Changes

The original problem definition required that a test rig be designed and manufactured for testing of a labyrinth seal, in which the rig was to be capable of performing tests with a shaft rotation of 10,000 rpm. Initially, a electric servo motor, gearbox, and high speed bearings were determined to be the most appropriate method for creating this amount of rotation, but during the design phase, it was determined that achieving rotation through this method was far beyond the budget provided for this project. Therefore due to the budget concerns, members of the project team and members of Danfoss Turbocor decided to remove this requirement from the test rig. The rig design would still include a shaft which had capabilities of rotation, but the rotation would only be used as a method for determining concentricity. Removal of this requirement, eliminated the need for an electric motor and a gearbox, but a form of bearings would still be needed to support shaft rotation.

The use of bearings created some concerns among members of the team about the ability to maintain a seal within the low pressure housing, and with the requirement for high speed rotation removed, the initial concept of utilizing bearings could be reevaluated. Danfoss Turbocor's manufacturing division recommended that bushings should replace the bearings, and they also provided examples of projects where this application had been implemented. It was determined that bushings would provide greater sealing capabilities through use of o-rings, and the bushings would also allow the shaft to be aligned with far greater ease. After evaluating the design change, members of the team decided it was a good decision to have the brass bushings replace the axial and radial bearings found in the initial design.

A flow measuring system was required to meet one of the main goals described in the project definition, which was to measure flow rates through a labyrinth seal. The original design included a digital flow meter, but in order to choose the proper measuring equipment, an estimated flow range needed to be determined. Engineers at Danfoss Turbocor did provide the project team with an equation which modeled flow rates through a labyrinth seal, but the results achieved through use of this equation could not be verified, as they were based on experimental results which could not be directly

correlated to the type of test being preformed in this project. Significant time was devoted to analyzing the calculations and comparing them to the ranges measured by available flow meters, but the team had great difficulty identifying a flow meter which was capable of measuring an accurate flow rate within the range that was predicted by provided calculations. Digital flow meters that were considered for this project were very expensive as compared to the available budget, and it was decided that purchasing a flow meter of such high expense would not be a wise decision if the expected flow rates could not be verified.

At this point the team momentarily disregarded the use of a digital flow meter, and began pursuing other options. After researching numerous flow measuring techniques, the team decided explore the capabilities two similar measuring techniques: orifice and Venturi flow meters. Specifications were found through different sources, and when the team had collaborated on which designs would best suit the application, manufacturing of these devices began. Both designs were manufactured within a reasonable time frame, and testing of each design followed shortly after their completion. However, it was determined that both designs would require calibration, which could not be preformed without an accurate flow meter. Manufacturing these devices was helpful for the teams understanding of flow measuring equipment, but would not provide a successful solution for measuring flow rates for this project.

It was determined that the team needed a method for measuring high flow rates, but it was also required that this method be easily adaptable to wide range of flow rates. The solution that appeared in the final design was the use of a converging nozzle located on the low pressure housing. Converging nozzles are used to determine flow rates through use of pressure ratios, and the relationship between Mach number. This proved to be an excellent solution to the flow measuring problem, as the range of flow rates could be adjusted at little expense, and the pressure measuring equipment had already been acquired. Initially pressure measurements were to be recorded using pressure transducers and software acquired through Danfoss Turbocor, but upon initial testing of this equipment, it was determined that readings collected from the transducers were not providing accurate results when measuring atmospheric pressure. In order to proceed

with testing, analog pressure readings would be utilized to acquire the data used in calculations of flow rate.

One of the requirements of this design project was to include a method for adjusting the concentricity of the seal in regards to the shaft. Initially, the team explored options to include a device which was labeled the “Differential Threading Mechanism”. A prototype of this device was manufactured, and the results of which proved to be successful. However, members of the Danfoss Turbocor manufacturing division recommended the use of micrometer heads, which would deliver the same results. Micrometer heads were available at low cost from an established supplier, and were easily adapted to the current rig design.

Initially, the concentricity of the seal was to be measured through use of a dial gauge. Ideally, this gauge would measure the location of the seal in relation to the shaft. This would be preformed by attaching the dial gauge to the shaft via magnetic base attachment which included adjustable arms. The adjustable arm would allow the dial gauge to measure almost any position on the rig, and it was decided that it would measure the inside of the seal. However, it was seen that the measurements taken with the dial gauge were not providing readings which were useful in determining concentricity. Instead, a similar measuring device was used, but with a different methodology in place. The seal would be aligned fully a-concentric (seal has made contact with the balancing piston), and then an electronic dial gauge would be set up 180 degrees offset from the direction in which the micrometer head would be creating displacement of the seal. The micrometer head would be used to move the seal until the contact was made with the opposite side of the seal. The gap size would be known from the reading taken on the dial gauge, and therefore, the concentric location could be determined and achieved. In order to achieve concentricity, it would be required to perform this alignment method twice, to achieve a concentric location along two axes. This method for achieving a concentric position of the seal was discussed in the early stages of the design process, but was eliminated due to concerns of accuracy. The concern of accuracy will be addressed by measuring the repeatability of this method, by performing multiple tests and averaging the results.

8. Manufacturing and Final Product

With the design for the labyrinth seal test rig finalized and the raw materials on order, manufacturing plans were loosely constructed around the project sponsor's machine shop labor schedule. The shop supervisor at Danfoss-Turbocor was not contacted until raw materials began arriving in mid-January, 2009. A meeting was held to introduce the design team members to the shop supervisor Robert Parsons, who has over 25 years shop experience. Mr. Parsons proved to be an invaluable asset in the manufacturing process. He revealed the difficulties in achieving the level of tolerances we had originally specified, and offered many shortcuts that would save time and money in manufacturing. Of the major changes, Rob Parsons suggested that the bearings be replaced with brass bushings, and that the team order micrometer heads instead of building differential threaded mechanisms to adjust the concentricity of the seal.

The majority of the manufacturing was conducted at Danfoss-Turbocor. The raw materials were delivered to the shop crew along with engineering drawings. As the parts were machined, members of the design group regularly visited to check the timing of the work. On several occasions the shop crew would find areas to advise, such as putting open tolerances on the connection between the shaft and bushings. The shop crew continuously critiqued and asked questions in an effort to ensure the success of the project.

The bottom mounting plate was the first part to be completed. The components to be welded to form the high and low-pressure vessels followed, and were welded. Unfortunately, the welded parts warped severely and additional machining was necessary to bring them back to within acceptable tolerances. This contributed to a time delay in the design team receiving the finished parts for assembly. The four ports in the high-pressure vessel and the four ports in the low-pressure vessel were machined after welding, as was the hole for the radial bearing in the low-pressure vessel. The radial bearing and the thrust bearing were machined from brass material at about the same time. The spacer bars were the last parts to be machined by Danfoss-Turbocore before timing became an issue. At that point the remaining parts were machined by the design team at an outside lab. The remaining parts originally scheduled to be machined by Danfoss-Turbocore that were

machined by the design team included the legs or the test rig and the shaft. Once these remaining parts were completed, assembly was able to begin.

The legs and spacers were connected to opposite sides of the bottom plate. The low-pressure vessel was connected to the spacers. The brass bushings were installed in their respective holes: the thrust bearing into the bottom plate and the radial bearing into the low-pressure vessel. O-rings were placed on the shaft, and the shaft was inserted through the bearings. The shaft was test-spun successfully. O-rings were installed in the labyrinth-seal mounting plate and the mounting plate was installed on the test rig. All o-rings were given a light coating of vacuum grease. The high-pressure vessel was then fitted over the labyrinth-seal mounting plate and the bolts connecting the two pressure vessels were tightened. All holes were properly fitted with NPT plugs, and the test rig was connected to "shop air" through PVC tube and a pressure regulator. The rig was pressurized and leak checked

Figure 20: Picture showing the high pressure vessel separated from the reat of the rig

with a bubble solution. A submersion-type test was also used to check for leaks. Many leaks were found to occur at the weld sites, and an attempt was made to seal the leaks with epoxy. The seal attempt was successful in that the rig was found to drop from 75 to 70 psi across ten minutes; the mass flow rate from the leak would be unable to compete with the massive flow rate through the labyrinth seal.

Instrumentation for the rig was assembled next. The plugs used to verify the absence of leaks were removed and replaced with temperature and pressure gauges. A nozzle was connected to the low-pressure vessel as a crucial part of measuring the flow. The 100-psi pressure relief valve was installed on the high-pressure vessel. The regulator was removed and a hose to connect with Danfoss-Turbocore's shop air supply was

installed in its place. All threaded connections to the pressure vessel were wrapped with a thin layer of Teflon tape. Teflon tape, more commonly known as “pipe tape” plays a crucial role in ensuring leak protection in fittings. For this reason it was necessary to reapply it whenever a fitting was removed.

In order to verify proper operation of the rig, the team was originally to conduct tests on multiple labyrinth seals. Due to time constraints, the machine shop at Danfoss-Turbocor was unavailable to machine the seals or the necessary displacer pistons (the part that fills in the space within the labyrinth seal, most often a shaft) and riser collars needed to test multiple designs of labyrinth seal. As discussed previously (see Design Changes, Section 6) a single seal would be used and teeth would be manually removed from it. To implement this change a displacer piston was needed. The displacer piston for the seal came from the seal’s intended displacer piston, a shrouded impeller. Fluid is intended to pass through the interior of the impeller while a seal is maintained around the circumference by the labyrinth. The interior of the shrouded impeller was covered with a large, aluminum flange washer that was custom-machined by the design team and the flange washer was sealed in place with epoxy. The impeller was then installed onto the shaft. The labyrinth seal was mounted in an aluminum adaptor designed to bridge the design of the seal with the design of the test rig. The seal between the labyrinth seal and the adaptor was made using epoxy, and the adaptor sealed to the rig through an o-ring connection. The adaptor was held in place with screws.

Figure 21: Seal in adapter plate and displace piston.

With the labyrinth seal and displacer piston installed, the rig was ready for tests. The high-pressure chamber was replaced over the labyrinth seal mounting plate, and the bolts holding the vessels together were installed and tightened after the concentricity property of the seal and displacer piston was adjusted. The hose from the high-pressure

vessel was connected to shop air supply and tests were conducted. Results of the tests can be found in a later section.

9. Testing Methodology

In designing a procedure in which to use the test rig, several criterions needed to be met in order for the testing process and the design to be considered a success: The testing seal needed to be interchangeable, the shaft-seal concentricity needed to be variable, and finally, an adequate high-to-low pressure ratio needed to be maintained. If all of the criteria are met, the recorded pressures can accurately be used to determine the flow rates through the seal.

According to the project scope the rig is required to test labyrinth seals from different stages of the standard Turbocor compressor. This means that the potential test seals' outer geometries are not all identical. Attaching a seal for tests requires an adapter plate that each individual seal must be mounted to. The adapter plates must be made individually to fit each seal size. The seal is mounted to its adapter plate through use of epoxy. This allows all of the seals to have a standard outer geometry that can easily be placed in between the two pressure chambers.

Due to time restrictions and manufacturing complications this project only tested one seal. Also, the seal provided was not one of the original four seals for which theoretical calculations had been made. In order to perform an analysis on the effectiveness of teeth in the labyrinth seal's ability to stop flow, after each test is performed, the seal was placed in a lathe so that a single tooth may be removed. The tooth was taken from the exit side of the seal. The tests were then repeated at the new tooth number. The seal originally had eight teeth, and tests were performed removing a single tooth each time until only 4 teeth remained. While this is not the original testing plan, it is believed that by removing teeth, an analysis can still be performed on the tooth effectiveness.

Figure 22: Profile view of the magnet dial gauge attached to the test rig for concentricity measurements.

During testing, once the seal had been securely placed in the test rig the concentricity could be altered. The project scope requires that each seal be tested concentrically and non-concentric, or off-centered. This

measure of concentricity was to be done by use of a dial gauge while micrometer heads could be used to make minute placement adjustments. The dial gauge was mounted on the shaft. The gauge itself extended to an outer edge of the seal. Rotation of the shaft indicated a displacement of the shafts axis to the seals. Although this method had been carefully studied and planned, it did not, unfortunately, work as intended. The validity of the dial gauge readings was unknown and it also was not possible to repeat the exact concentric movement. A new methodology for varying concentricity was formed. The rig was placed on its side with the screws attaching the seal adapter plate to the rig as loose as possible. This allowed the plate to be moved downward in the negative y direction easily. By placing the rig on its side, gravity served as a check that the seal was in the most un-concentric position possible (the seal and shaft touching). With a micrometer head placed at that bottom location on the seals outer edge, movement of the seal in "upward" direction was achievable. The rig was then placed upright and the movement was made. Using the dial gauge on the opposite side and the micrometer head for movement, a maximum displacement was measured. Half of that distance was considered to be the center of the hole. The same process was done in the "x" direction when the rig is tipped over horizontally. By performing the movements in both the x and y planes, it can be assumed that the shaft is centered with respect to all sides of the seal. This method is not as exact as the intended plan but it is repeatable and gives a concentric result. Tests were performed at the completely non-concentric position and the concentric position.

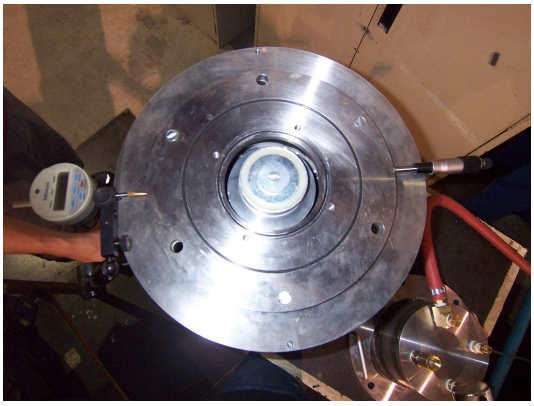

Figure 23: top view of the test rig showing the micrometer and pressure gauge in parallel positions for concentricity movement.

Once the seal had been placed in the intended orientation around the shaft and secured, the high pressure vessel could be bolted back onto the test rig. At this point, the rig is considered ready to be used for testing. A test consisted of turning on the air supply until a minimum pressure inside the high pressure vessel is reached. The pressure can then be increased and pressure reading should be taken from both the high and low pressure values at each new pressure level. Unfortunately, through the course of testing,

it was found that supplying the minimum pressure was difficult. To allow for versatility, the test rig was designed to be used with either shop air or a compressed air cylinder. Out of convenience, the first test was performed using shop air at the High Magnet Field Lab's Shaw building. Unfortunately, the shop air was not able to provide the necessary pressure high pressures; the maximum pressure recorded in the high pressure vessel was 10 psig. A switch was made to compressed air which yielded slightly better results, 30 psig, but the pressures were still lower than desired and were severely limited by the amount of air available in the gas cylinder. After consulting with the machinist at Danfoss-Turbocor, it was discovered that the issue lay not in the air source, but in the supply lines. Due to the size of the connections between the air supply and the pipeline to the test rig, air was bottlenecking, preventing the needed flow rates from reaching the rig. A solution was found by using the shop air at the machine shop of Danfoss-Turbocor. The machine shop was able to supply higher pressure shop air and better connections that allowed a higher pressurization of the test rig to take place. While this solution did limit when testing could be done, the tests were completed on schedule and without further issue.

10. Test Results and Analysis

Figure 24: An assembled view of the rig, taken during testing

The testing procedure described in the previous section was utilized in conjunction with the test rig to collect data on the behavior of fluid as it flows through a labyrinth seal, specifically how various conditions affect the mass flow rate. To that end, two tests were conducted per tooth number, a concentric test and a non-concentric test. During testing the high pressure vessel was used regulate the flow into the rig and pressure measurements were taken in increments of 5psig starting from 10 psig (0.177 MPa) and going up to 40 psig (0.377 MPa). As previously discussed, the electronics that were originally intended for data

collection were malfunctioning, leading to an alternative method of data collection and mass flow analysis. Using analog pressure gauges, the pressures of both pressure vessels were recorded. These numbers were used to form a ratio that could be used in the theoretical flow calculations by Egli outlined in Section 4. To determine the actual flow rate through the seal, equations that model flow through a converging nozzle were used. The equations rely on relationships that are often used in calculating mach numbers, and were so termed "Mach number relations". The methodology for calculating the mass flow out of the seal is outlined below and a sample calculation of this method is available in Appendix A.2.

$$P_L = P_e\left(1+\frac{\gamma-1}{2}M^2\right)^{\frac{\gamma}{\gamma-1}} \qquad (10)$$

Generically, Equation 10 defines the static pressure inside a container in terms of the exit pressure, ratio of specific heats ($\gamma = C_p / C_v$), and the Mach number. It should be noted that this relationship will hold true even though sonic flow is never reached. Through manipulation, Equation 10 can be used to solve for the Mach number in terms of the ratio of $Pr = P_L : P_e$ (low pressure vessel: exit pressure) and γ.

$$M = \sqrt{\left(P_r^{\frac{\gamma-1}{\gamma}}-1\right)\frac{2}{\gamma-1}} \qquad (11)$$

$$V = M\sqrt{\gamma RT} \qquad (12)$$

From here, the Mach number can be used to determine the velocity of the flow (Equation 12), which can then be multiplied by the area of the nozzle and the fluid density to determine the mass flow rate. The results of these calculations are all available in Appendix B.3. It was this method of calculation that was used to bring about the results discussed in sections 9.1 and 9.2.

Before discussing the results, the propagation of error that is associated with these calculations should be made note of. The contributing measurements that carry with them an instrumental limit of error are: the pressure (ILE=0.25 psig = 1724 Pa), Diameter of the nozzle (ILE=0.013 mm), and the ambient room temperature (ILE=1^0C). To determine the calculation of error the following equation was used

$$m_{error} = m_{flow}\sqrt{\left(\frac{P_{error}}{P_L}\right)^2\left(\frac{D_{error}}{D}\right)^2\left(\frac{T_{error}}{T}\right)^2} \qquad (13)$$

Using Equation 13 the propagation of error was determined for all mass flow rates. A sample calculation is available in Appendix A.3. The average of the mass flow rates was found to be plus or minus 9.34×10^{-7} kg/s. The error is small enough that the error bars on the graphs are not noticeable. Due to the small error calculated for the mass flow rates, analysis can proceed with certainty that the results are significant and are not within the instrumental limit of error.

10.1 Relationship between tooth number and mass flow rate

One of the driving motivators for this project is to determine the relationship between tooth number and flow rate through a seal. Based on the how a labyrinth seal works, it was believed that removing teeth from the seal would decrease its effectiveness by allowing more fluid to pass through. To determine if this was the case the mass flow rates for each tooth number were calculated and plotted as a function of the pressure as can be seen below is Figure 25

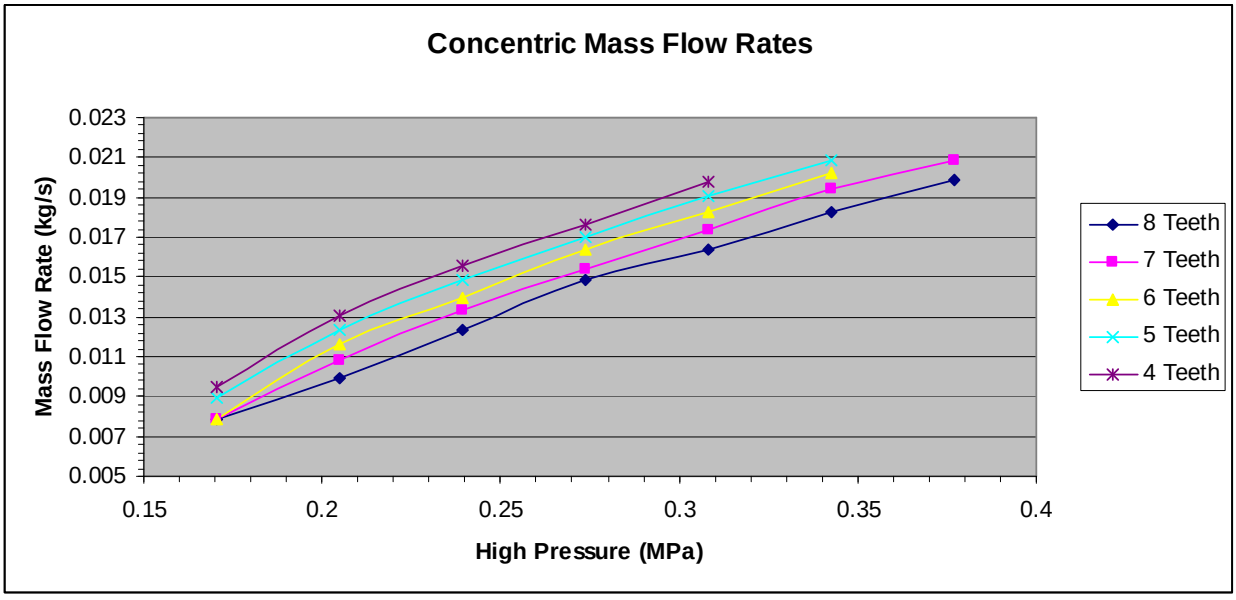

Figure 25: Graph of the calculated mass flow rates through the seal as a function of the pressure on the high side. These are the calculated results for all tooth tests performed under the concentric condition.

As can be seen in the graph above, the flow rate behaved as expected and did increase as the number of teeth in the seal was reduced. In addition to confirming the expected trend, there are some other interesting features in the graph worth noting. To begin, it can be seen that there are less data points for tests conducted at 6, 5, and 4 teeth. This is, not because these pressures were not run, but because at these pressures the flow that was allowed through the seal exceeded the rig's measuring capabilities. It is believed that instrumentation with a larger range would be able to record the values. Despite the problems in instrumentation, the effect that removing just two teeth has on a seals ability to deter flow can easily be seen, especially at higher pressures.

A more subtle trend that can be seen in the above figure is that the increase in mass flow rates between each test is approximately equal at any given flow rate. For instance, the increase in flow rate from 6 teeth to 5 teeth is approximately equal to the increase when going from 5 teeth to 4 teeth. The obvious exception to this trend is seen in the data between 7 and 8 teeth. This particular tooth removal may have had a greater impact since it was the first tooth to be removed. This may have impacted the flow greater due to a machining difference that was then erased when the second tooth was removed, or more likely, because it was the tooth closest to the exit, it had the greatest impact on flow.

Another interesting trend is the impact that tooth removal has at varying flow rates. In Figure 25 it can be seen that while the lower tooth numbers have higher flow rates in general, at lower pressures the flow rates are much closer together. As the pressure above the seal is increased the lines for each tooth flow rate separate and no longer have flow rates clustered together. Essentially, tooth removal has a greater impact on the flow rate at higher pressures. The graph below attempts to illustrate this effect by plotting the average mass flow increase at different pressures caused by removing a single tooth.

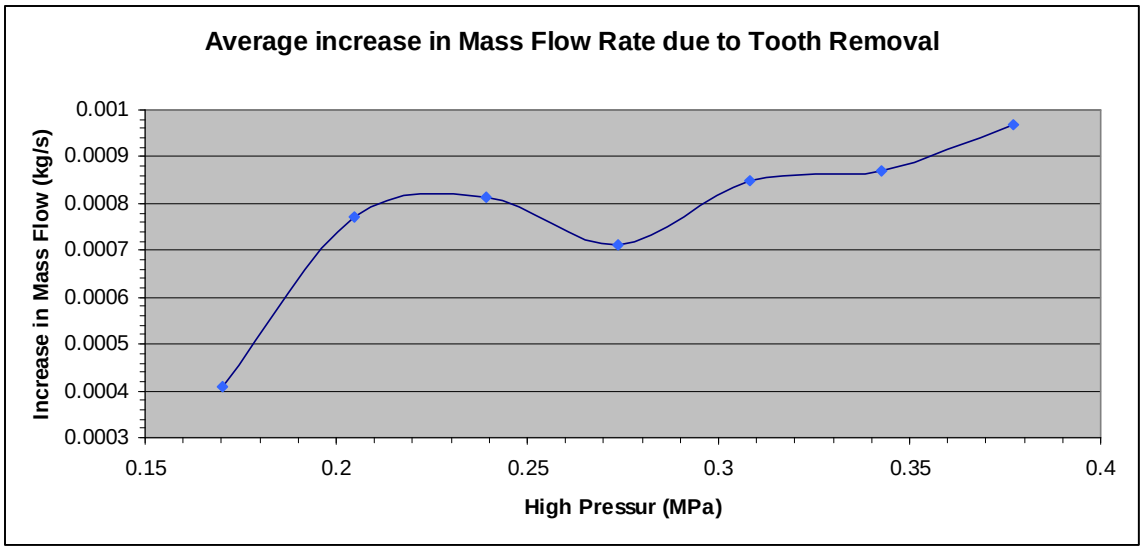

Figure 26: The graph was created by finding the difference in flow rates between each tooth at individual pressures. The data that has been plotted represents the average increase at each pressure.

While Figure 26 does not show a linear increase, it does confirm the general trend that tooth removal plays a greater effect at higher pressures due to the overall increasing trend seen in the flow rate differences. What this means is that at higher pressures, the removal of one tooth will cause a larger increase in leakage through the seal than it would at low pressures.

10.2 Relationship between concentricity and mass flow rate

Another relationship that the engineers at Danfoss-Turbocor were interested in determining is the relationship between concentricity and flow rate. To determine what relationship, if any, existed tests were run at the two most extreme concentricity conditions: Completely non-concentric (The seal and shaft are touching), and perfectly concentric (as close to centered as was possible). After analysis and comparison of the flow rates between the concentric tests and non-concentric tests that concentricity does indeed have an effect, although it is relatively minor. When comparing flow rates of the same tooth number and different tests it was found that the non-concentric at best had no effect and at worst increased the flow rate. The graph below shows the average increase in leakage through a seal due to non-concentricity.

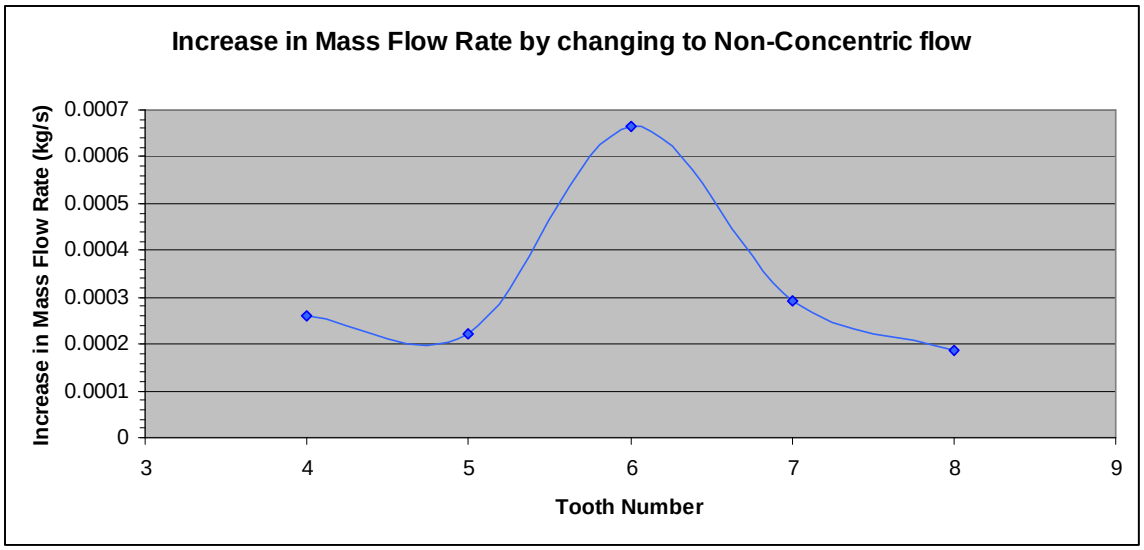

Figure 27: Plots the average increase in leakage through a seal as a function of the number of teeth. The data was calculated by subtracting mass flow rates of the concentric tests from the non concentric tests and averaging the values for each tooth count.

When looking at the graph the most obvious feature is the dome like shape that is formed. This trend can be interpreted as changing concentricity effects mass flow only up to a certain point, after which it is more likely that mass flow rates will be impacted more heavily by other factors such as the number of teeth. It can be seen that non-concentricity had the greatest effect when the seal had 6 teeth and the least effect when the seal had 8 teeth. To compare the data, graphs of mass flow rates with respect to pressure are available in Figures 28a and 28b. All of the concentricity graphs are available in Appendix B.5

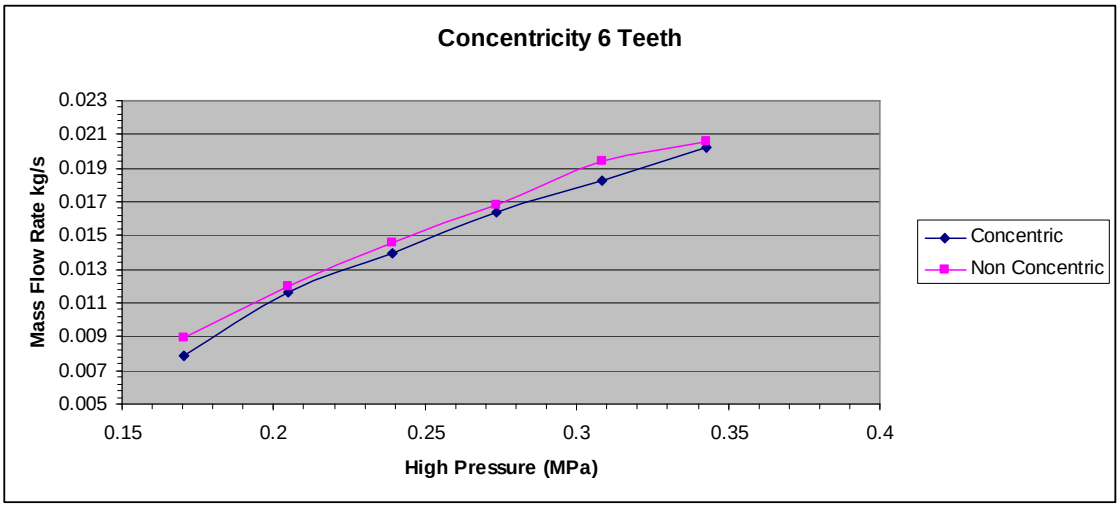

Figure 28a: Plots the mass flow rates of both the concentric and non-concentric tests for 6 teeth as a function of pressure.

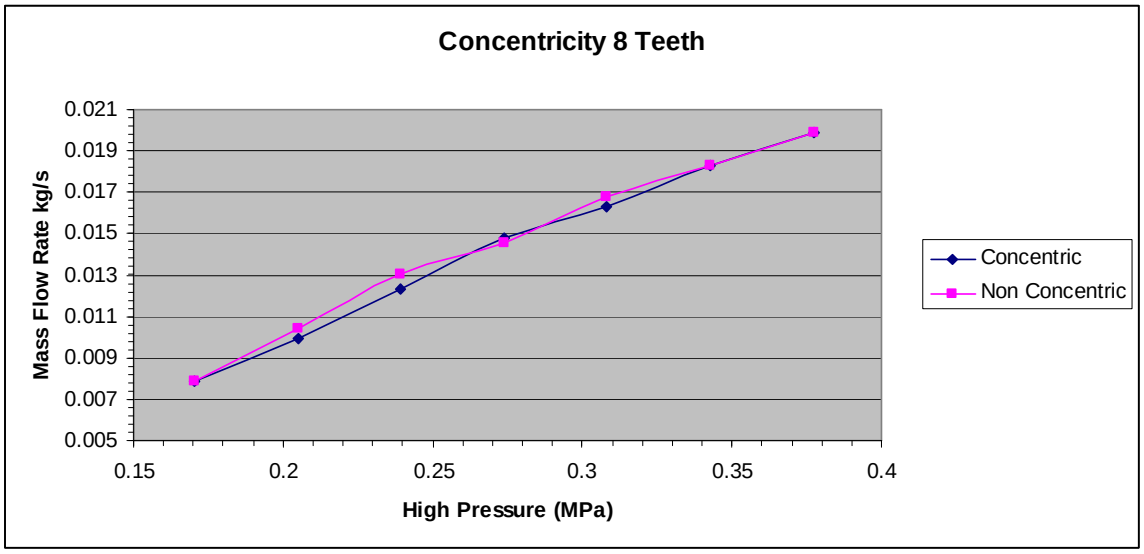

Figure 28b: Plots the mass flow rates of both the concentric and non-concentric tests for 8 teeth as a function of pressure.

The first thing that is noticed when comparing the two graphs is that mass flow rates for the two tests are identical at three separate pressures, and very close on one more. In fact, there are only two points where concentricity had a sizeable impact (at P=0.205 and P=0.239 MPa). The data for tests run at 6 teeth, however, presents two distinct lines where the non-concentric flow rates are much higher than the concentric flow rates. It does not appear that the effect of concentricity varies with pressure.

The tests have proved that concentricity does have an effect on flow rates, however, it is not a sizeable one. If machining costs needed to be reduced concentricity could be sacrificed to a small extent with little impact on the performance of the seal. However, despite the relatively small impact that non-concentricity has on the leakage, it is still the belief of the designers that concentricity should be maximized to the best of machining ability. In addition to improving seal performance, concentric conditions will reduce wear on the seals and shafts that would otherwise occur in non-concentric conditions. Finally the effect of non-concentric conditions has on leakage rates may be increased if the shaft were spinning.

10.3 Differences between theoretical and actual flow rates

As mentioned at the beginning of this section, the mass flow rates were not able to be directly measured and so they needed to be found indirectly through use of Mach number relations for flow through a nozzle. Finding flow rates through relationships rather than measuring directly is generally considered to be less accurate since the results are now relying on correct calculations in addition to the values which are already being measured. However, being forced to use relations rather than direct measurement did introduce another avenue for more in depth analysis on the behavior of flow through labyrinth seals. When the predicted flow rates using the Egli relations were compared to the actual flow rates found using the Mach relations, the actual flow rates were considerable higher, usually by a factor of 10 and sometimes higher.

There are several possible explanations as to why there is such a large difference between the theoretical values and the actual values. To begin, the Egli relations are designed to predict flow rate inside a labyrinth seal. The Mach relations, however, are designed to predict flow exiting a nozzle into ambient conditions. The construction of the relations due to their different purposes introduces several fundamental differences. For instance, the Egli equations are more strongly influences by the actual seal geometry than fluid conditions. In fact, all of the fluid properties are taken from conditions on the high pressure side of the seal. By relying more on geometry, this gives the Egli relations the ability to be used on all labyrinth seals with any number of teeth. The Mach number relations are very different in that the only geometry they take into account is the exit area of the nozzle, and that is only to use the generic mass flow formula $m_{dot}=\rho VA$. The properties of both conditions inside the vessel and ambient conditions are used to determine flow behavior.

An interesting thing to note is that while both relations make use of pressure ratios, Egli using $P_L:P_H$ and Mach using $P_L:P_e$, the ratios are inverted. The pressure ratio in the Egli formulas will always be greater than 1 while the Mach ratios will (in the subsonic case that applies to this experiment) always be less than 1 since the pressure inside the test rig should be greater than atmospheric pressure. It is unknown as to whether or not this inverted ratios had any effect on the results, but since the proper procedures for both models were used, it is assumed to be negligible.

Finally, it should be noted that the Egli relations make use of experimentally determined coefficients. Since the experiments that were performed to determine these coefficients were performed without the test rig in mind, they should be used with care and the understanding that there is an error inherent in any such relation. Despite the differences in theoretical and actual flow rates, the tests are considered successful and the results as reliable as possible given the instrumentation constraints. The test rig was modified so the low pressure vessel was draining through a converging nozzle making the Mach number relations applicable to the tests. While more tests with varying seal sizes should be performed for a more complete analysis, the test rig was able to confirm that leakage through a seal will increase as the tooth number is decreased. Concentricity was also proven to have an impact, albeit minimal.

11. Future Work

Certain aspects of this project were left incomplete due to time and budget limitations, and for a complete understanding of the leak rate through a labyrinth seal, further testing is required. The main aspect of the project which needs to be revisited is the rotational component of the shaft. Utilizing a rotating shaft during testing should show a decrease in flow rates through the seal, but it is unknown what type of changes will be encountered by removal of teeth with the rotational component included. The current test rig can support a rotational shaft, but some retrofits would be required in order to meet this goal. The first change required would be in the addition of high speed bearings. The axial load bushing could remain in place, as it serves as a method for shaft alignment, but machining would be required to secure the bearings to the bushings. Originally the rotational component of the test rig was removed due to budget limitations, but upon further discussions with Danfoss Turbocor manufacturing division, the use of compressed air to drive the shaft could be implemented at low cost, while achieving the needed speeds. These two additions to the rig should meet the original rotational requirements.

Another issue discovered during testing deals with the concentricity measurements and adjustment. The initial method for concentricity measurement included utilizing a dial gauge connected to the shaft, and rotating the gauge while measuring the outside of the ring seal. However, the results provided from this test were inconclusive, and required the team to devise a new method of testing. The failure of this test could be attributed to poor manufacturing of the ring which supported the shaft, or possibly a misalignment of the shrouded impeller with respect to the shaft. To alleviate these issues, more careful manufacturing of the adapter ring and shrouded impeller need to be taken.

The micrometer heads used on this rig were attached with a single screw, and therefore were free to rotate about the axis of the screw. Therefore, the direction of displacement for this device could not be guaranteed. For testing purposes, a digital dial gauge was utilized to measure the displacement along the axis of the micrometer head, but due the connection of the micrometer head, a true concentric location could not be achieved. Future work should address this issue, and constrain the micrometer heads to allow for only one direction of motion.

Finally, should more studies be performed using the test rig, it is recommended that more precise instrumentation be used. The original electronics supplied by Danfoss-Turbocor were not used due to a malfunction in one of the pressure gauges making the readings inaccurate. The transducer should be replaced so that more accurate reading are available. Also investment in a high end flow meter would be able to provide definitive results as to the amount of flow going through the seal. Measurements taken using a flow meter could be compared to both the Egli theoretical mass flow relations and the mass flow rate found through use of “Mach-number” relations through a nozzle. This would provide a more complete range on the analysis of flow behavior through a labyrinth seal.

References & Vendors

Sources

- Author Unknown "Centrifugal Compressors" Chapter 4: Pg 62-66
- Childs, Peter R. Mechanical Design Pg 184. Arnold Publishers © 1998
- Dr. Egli Classical Concepts and Papers on Labyrinth Seals. 1935
- http://www.engineeringtoolbox.com/friction-coefficients-d_778.html
- Hibble, R. C. Engineering Statics and Mechanics. 2nd Edt. Upper Saddle River: Prentice Hall, 2002. NJ 07458
- John, James & Keith, Theo. Gas Dynamics 3rd Edition Chapter 3 Pg 83-89. Prentice Hall, 2006. NJ 07458
- Norton, Robert L. Machine Design : An Integrated Approach. 3rd ed. Upper Saddle River: Prentice Hall, 2005. 609-20.
- Piotrowski, John. Shaft Alignment Handbook. Danbury: NetLibrary, Incorporated, 1995.
- http://www.portlandbolt.com/technicalinformation/astm/ASTM_A307.html
- http://www.scottecatalog.com/scotttec.nsf/74923C9EC562A6FB85256825006EB87D/EF6A526EB60A3C8785256A2C0040B17E?OpenDocument
- http://www.skf.com/skf/productcatalogue/jsp/viewers/productTableViewer.jsp?&imperial=false&lang=en&newlink=1&tableName=1_1_1&presentationType=3&startnum=16
- http://www.vxb.com/page/bearings/PROD/Kit7437?gclid=CNjThKX_nZcCFQJvswodVUaj9g

Vendors

- http://www.metalsdepot.com
- http://www.drillspot.com/products/376896/Approved_Vendor_5MY72_Low_Carbon_Steel_Threaded_Rod
- http://www.omega.com

- http://www.shender4.com/thread_chart.htm

Appendix 1: Sample Calculations

A.1: ***Calculation of mass flow rate using the Egli relations for both air and R134a as the working fluid***

A.2: ***Calculation of mass flow rate using the Mach number relations***

A.3: ***Calculation of the propagation of error in the Mach number relations***

A.4: ***Calculations performed for the loading inside the pressure vessels***

A.5: ***Calculations performed for the bearing load analysis***

A.6: ***Calculations performed for the proof of concept prototype***

Appendix A.1: Egli relations for air

Egli Relations using Test Results
N=8 teeth , Concentric
Working Fluid: AIR

Nomenclature:

Cc = Empirical coefficient
Cr = Empirical coefficient
Ct = Empirical coefficient
Af = Flow Area
T = Temperature (high P side)
t = Tooth thickness
N = number of teeth
P = Pressure
Pr = Pressure ratio
p = Tooth spacing
R = Gas Constant
Re = Reynolds Number
r = radius
= gap diameter
= density (high P side)

Governing Equations:

$$m_{dot} = \pi \cdot 2 \cdot r_o \cdot \delta \cdot C_t \cdot C_c \cdot C_r \cdot \rho_o \cdot \sqrt{R \cdot T} \qquad m_{dot} = \rho A V$$

$$C_t = 2.143 \frac{\ln(N) - 1.464}{n - 4.322} \cdot \left(1 - P_r\right)^{0.375 \cdot P_r} \qquad R = C_p - C_v$$

$$C_r = 1 - \frac{1}{3 + \left(\frac{54.3}{1 + 100 \cdot \frac{\delta}{t}} \right)^{3.45}} \qquad C_c = 1 + X_1 \cdot \frac{\frac{\delta}{p} - X_2 \cdot \ln\left(1 + \frac{\delta}{p}\right)}{1 - X_2}$$

$$A = \pi\left(r_o^{\,2} - r_i^{\,2}\right) \qquad Re = \frac{\rho V D}{\mu} = \frac{V D}{\nu}$$

$$X_1 = 15.1 - 0.05255 e^{0.507 \cdot (12 - N)} \qquad X_2 = 1.058 + .0218 N \qquad N < or = 12$$

$$X_1 = 13.15 + .1625 N \qquad X_2 = 1.32 \qquad N > 12$$

Appendix A.1: Egli Relations for air

Seal Dimensions: Impeller Labyrinth Gap size .18mm

$r_o := \frac{68}{2}mm$ $p := 1mm$ $\delta := 0.18mm$ $t := .5mm$ $N_{teeth} := 8$

ro is the inner diameter of the seal but the outer diameter of the teeth

$r_i := r_o - \delta$

$A_{flow} := \pi \cdot \left(r_o^{\,2} - r_i^{\,2} \right)$ $A_{flow} = 38.351\,mm^2$

Air Properties at Testing Conditions

$kJ := 1000J$

$T_{hp} := (14 + 273.15)K$ $P_L := .1048MPa$ $P_H := .1772MPa$ $P_r := \frac{P_L}{P_H} = 0.591$

$\rho_o := 2.1484\frac{kg}{m^3}$ $C_p := 1.0076\frac{kJ}{kg \cdot K}$ $C_v := .71781\frac{kJ}{kg \cdot K}$ $\nu := .083540\frac{cm^2}{s}$

$R := C_p - C_v$

Appendix A.1: Egli relations for air

Mass Flow Calculation:

$$C_r := 1 - \frac{1}{3 + \left(\frac{54.3}{1 + 100\cdot\frac{\delta}{t}}\right)^{3.45}} \qquad C_r = 0.852$$

$$C_t := 2.143\frac{\ln\left(N_{teeth}\right) - 1.464}{N_{teeth} - 4.322}\cdot\left(1 - P_r\right)^{0.375\cdot P_r} \qquad C_t = 0.294$$

$$X_1 := 15.1 - 0.05255e^{0.507\cdot\left(12 - N_{teeth}\right)} \qquad X_1 = 14.701$$

$$X_2 := \left(1.058 + .0218 N_{teeth}\right) \qquad X_2 = 1.232$$

$$C_c := 1 + X_1\cdot\frac{\frac{\delta}{p} - X_2\cdot\ln\left(1 + \frac{\delta}{p}\right)}{1 - X_2} \qquad C_c = 2.517$$

$$m_{dot} := \pi\cdot 2\cdot r_o\cdot\delta\cdot C_t\cdot C_c\cdot C_r\cdot\rho_o\cdot\sqrt{R\cdot T_{hp}} \qquad m_{dot} = 0.015\frac{kg}{s}$$

Appendix A.1: Egli relations for R134a

Theoretical results
N=8 teeth Concentric
Working Fluid: R134a

Seal Dimensions: Impeller Labyrinth Gap size .18mm

$r_o := \frac{68}{2}mm$ $p := 1mm$ $\delta := 0.18mm$ $t := .5mm$ $N_{teeth} := 8$

ro is the inner diameter of the seal but the outer diameter of the teeth

$r_i := r_o - \delta$

$A_{flow} := \pi \cdot \left({r_o}^2 - {r_i}^2 \right)$ $A_{flow} = 38.351\,mm^2$

Air Properties at Testing Conditions

$kJ := 1000J$

$T_{hp} := (14 + 273.15)K$ $P_L := .1048MPa$ $P_H := .1772MPa$ $P_r := \frac{P_L}{P_H} = 0.591$

$\rho_o := 7.9051\frac{kg}{m^3}$ $C_p := .85332\frac{kJ}{kg \cdot K}$ $C_v := .75106\frac{kJ}{kg \cdot K}$ $\nu := .014366\frac{cm^2}{s}$

$R := C_p - C_v$

Appendix A.1: Egli relations for R134a

Mass Flow Calculation:

$$C_r := 1 - \frac{1}{3 + \left(\frac{54.3}{1 + 100\cdot\frac{\delta}{t}}\right)^{3.45}} \qquad C_r = 0.852$$

$$C_t := 2.143\frac{\ln\left(N_{teeth}\right) - 1.464}{N_{teeth} - 4.322}\cdot\left(1 - P_r\right)^{0.375\cdot P_r} \qquad C_t = 0.294$$

$$X_1 := 15.1 - 0.05255e^{0.507\cdot\left(12 - N_{teeth}\right)} \qquad X_1 = 14.701$$

$$X_2 := \left(1.058 + .0218 N_{teeth}\right) \qquad X_2 = 1.232$$

$$C_c := 1 + X_1\cdot\frac{\frac{\delta}{p} - X_2\cdot\ln\left(1 + \frac{\delta}{p}\right)}{1 - X_2} \qquad C_c = 2.517$$

$$m_{dot} := \pi\cdot 2\cdot r_o\cdot\delta\cdot C_t\cdot C_c\cdot C_r\cdot\rho_o\cdot\sqrt{R\cdot T_{hp}} \qquad m_{dot} = 0.033\frac{kg}{s}$$

Appendix A.2: Mass flow rate using Mach number relations

Sample calculations are performed for 8 tooth concentric test, at .104 MPa

Nomenclature

PL = pressure in low pressure vessel
Pe = exit pressure
Te = exit temperature
γ = Cp/Cv
M= mach number
V = Velocity
ρ e = exit density
Ae = exit area of the nozzle
R = ideal gas constant of air
mdot = mass flow rat

Governing Equations:

$$P_L = P_e \cdot \left(1 + \frac{\gamma - 1}{2} \cdot M^2\right)^{\frac{\gamma}{\gamma - 1}}$$

$$a = \sqrt{\gamma \cdot R \cdot T} \qquad V = M \cdot a \qquad \rho = \frac{P}{RT} \qquad A = \pi r^2 \qquad m_{dot} = \rho A V$$

Variables

$\gamma := 1.4$ $\qquad P_L := 104804\,Pa$ $\qquad P_e := 101100\,Pa$ $\qquad P_r := \frac{P_L}{P_e}$

$R_{air} := 287\frac{J}{kg \cdot K}$ $\qquad T_e := 297.15\,K$

$D_{nozzle} := .008\,m$ $\qquad A_e := \pi \cdot \left(\frac{D_{nozzle}}{2}\right)^2$

Appendix A.2: Mass flow rate using Mach number relations

Calculation of mass flow rate from the low pressure vessel to atmosphere:

$$M := \sqrt{\left(P_r^{\frac{\gamma-1}{\gamma}} - 1\right)\frac{2}{\gamma - 1}} \qquad M = 0.227$$

$$a := \sqrt{\gamma \cdot R_{air} \cdot T_e} \qquad a = 345.536\frac{m}{s}$$

$$V_e := M \cdot a \qquad V_e = 78.542\frac{m}{s}$$

$$\rho_e := \frac{P_e}{R_{air} \cdot T_e} \qquad \rho_e = 1.185\frac{kg}{m^3}$$

$$m_{dot} := \rho_e \cdot A_e \cdot V_e \qquad m_{dot} = 4.68 \times 10^{-3}\frac{kg}{s}$$

Appendix A.3: Propagation of error through the Mach number relations

These are sample calculations to determine the error that is inherent in the mass flow rates calculated using the Mach number relations for flow through a nozzle

ILE

$P_{error} := .25 \cdot psi$ $d_{error} := .013 \cdot mm$ $T_{error} := 1$

Error in mass flow rate

The sample calculation is performed for the data corresponding to 8 teeth, concentric, at 10 psig (.1048 MPa)

$P_L := .1117 \cdot MPa$ $D := .008 \cdot m$ $T_{rig} := (25 + 273)$ $m_{dot} := 4.68 \cdot 10^{-3} \frac{kg}{s}$

Applicable Formulas:

$$A_{noz} = \pi \cdot \left(\frac{D}{2}\right)^2$$

$$M = \sqrt{\left(P_r^{\frac{\gamma - 1}{\gamma}} - 1\right)\frac{2}{\gamma - 1}}$$

Since Pr is a ration of internal pressure to atmospheric pressure, the only error is due to that of P, Pe, and γ are both considered constants

$$a = \sqrt{\gamma R T}$$

The temperature is that of ambient conditions

$$V = Ma$$

$$m_{dot} = \rho V A$$

The error in mass flow rate is effected by error in Pressure, Diameter, and Temperature, the rest of the variables are considered constants

$$m_{dot\_error} := m_{dot} \cdot \sqrt{\left(\frac{P_{error}}{P_L}\right)^2 + 2\left(\frac{d_{error}}{D}\right)^2 + \left(\frac{T_{error}}{T_{rig}}\right)^2}$$

$$m_{dot\_error} = 7.469 \times 10^{-5} \frac{kg}{s}$$

Appendix A.4: Pressure Vessel Analysis Calculations

Nomenclature:
σ 1: Hoop Stress, or the stress in the circumerential direction
σ 2: Longitudinal Stress, or stress in the axial direction
τ : Tensile yield strength (of steel)
FS: Factor of Safety (for both hoop or longitudinal stresses)
t: Wall thickness
r: Inner radius
P: Guage pressure
Subscripts
hp: High pressure (side)
lp: Low pressure (side)
act: actual pressure
atm: atmospheric pressure

Governing Equations:

$$\sigma_1 = \frac{P \cdot r}{t}$$

$$\sigma_2 = \frac{P \cdot r}{2t}$$

$$FS_1 = \frac{\tau}{\sigma_1}$$

$$FS_2 = \frac{\tau}{\sigma_2}$$

$$P_{guage} = P_{act} + P_{atm}$$

Tensile Strength of A36 Steel

$$\tau := 400 \cdot 10^6 Pa$$

Appendix A.4: Pressure Vessel Analysis Calculations

High Pressure Side:

Dimensions & Pressures:

$d_{hp} := .25in$ $\quad P_{atm} := 101.3 \cdot 10^3 Pa$ $\quad P_{act} := 400 \cdot 10^3 Pa$

$r_{hp} := \frac{d_{hp}}{2} = 0.07m$ $\quad P_{hp} := P_{act} + P_{atm} = 5.013 \times 10^5 Pa$ $\quad t_{hp} = 0.25 in$

Stress Calculations

$$\sigma_{1\_hp} := \frac{P_{hp} \cdot r_{hp}}{t_{hp}} = 5.514 \times 10^6 Pa \qquad \sigma_{2\_hp} := \frac{P_{hp} \cdot r_{hp}}{2 \cdot t_{hp}} = 2.757 \times 10^6 Pa$$

$$FS_{hp1} := \frac{\tau}{\sigma_{1\_hp}} = 72.539 \qquad FS_{hp2} := \frac{\tau}{\sigma_{2\_hp}} = 145.077$$

Low Pressure Side:

Dimensions & Pressures:

$d_{lp} := 5.5in$ $\quad P_{Lp\_act} := 101.3 \cdot 10^3 Pa$ $\quad P_{atm} = 1.013 \times 10^5 Pa$

$r_{lp} := \frac{d_{lp}}{2} = 0.07m$ $\quad P_{lp} := P_{Lp\_act} + P_{atm} = 2.026 \times 10^5 Pa$ $\quad t_{lp} := .25in$

Stress Calculations

$$\sigma_{1\_Lp} := \frac{P_{lp} \cdot r_{lp}}{t_{lp}} = 2.229 \times 10^6 Pa \qquad \sigma_{2\_Lp} := \frac{P_{lp} \cdot r_{lp}}{2 \cdot t_{lp}} = 1.114 \times 10^6 Pa$$

$$FS_{Lp1} := \frac{\tau}{\sigma_{1\_Lp}} = 179.485 \qquad FS_{Lp2} := \frac{\tau}{\sigma_{2\_Lp}} = 358.97$$

Appendix A.5: Bearing Load Analysis calculations

Ball Bearings

$rev := 2\pi\ rad$ $\omega := 10000\frac{rev}{min}$ $t := 10hr$

$\omega = 1.047\times 10^{3}\frac{1}{s}$

Solving for the lifetime of the bearings in millions of revolutions using the rotation speed and time

$L_{10} := \frac{t\cdot\omega}{10^{6}}$ $\boxed{L_{10} = 6\cdot rev}$ Life in millions of revolutions

Load

$D_{piston} := 4in$ $kPa := 1000Pa$ $P_{max} := 100psi$ $P_{max} = 689.476kPa$

$A_{shaftedge} := \frac{\pi}{4}\cdot D_{piston}^{2}$

Used the pressure in the high pressure chamber to calculate the force exerted on the shaft and piston surface

$A_{shaftedge} = 8.107\times 10^{-3}m^{2}$

$F_{pressure} := P_{max}\cdot A_{shaftedge}$

$37.1mm = 1.461\cdot in$

$F_{pressure} = 5.59\times 10^{3}N$

$D_{shaft} := 1in$ $L := 9in$ $\rho_{A36} := 7800\frac{kg}{m^{3}}$

$V_{shaft} := \frac{\pi}{4}\cdot D_{shaft}^{2}\cdot L$ $V_{shaft} = 0.116L$

$m_{shaft} := \rho_{A36}\cdot V_{shaft}$ $m_{shaft} = 0.903kg$ $g = 9.807\frac{m}{s^{2}}$

$W_{shaft} := m_{shaft}\cdot g$ $W_{shaft} = 8.86N$

Calculated the weight of the shaft by solving for the mass using the volume and density

$F_a := F_{pressure} + W_{shaft}$

$F_a = 5.599kN$

$F_r := 90N$

This value for radial load was chosen arbitrarily, it is because there is actually no net force acting on the bearing in the radial direction because it is going to be supported 360 degrees by low pressure chamber and supports.

Appendix A.5: Bearing Load Analysis calculations

$\frac{F_a}{V \cdot F_r} = 62.207$

According ot the value of e, e < or > this equation. The value for the variable 'V' is one because of a rotating inner ring in the bearing design (by choice). See page 618 of teh text "Machine Design" for a full explanation.

X := 0.5(

Since the above value is greater than e, the X and Y values are fixed to these values.

Y := Int(.42, 1.04, .56, 1.00, .602)

$Y = 0.988$

$F_e := X \cdot V \cdot F_r + Y \cdot F_a$

$\boxed{F_e = 5.582\,kN}$

The equivalent force with correction factors is solved for and can be used to calculate the final dynamic load.

$C_{final\_1} := F_e \cdot L_{10}^{\frac{1}{a}}$

$\boxed{C_{final\_1} = 18.716\,kN}$

The dynamic load is is within .6 percent of the bearing load and is an acceptable choice for our application.

Appendix A.6: Prototype Calculations

Test 2 - Operating Pressure: 3 psi

Gas constant for diatomic nitrogen: $R_{Nitrogen} := 0.3141 \frac{kJ}{kg \cdot K}$

Assumed Operating Pressure: $T := 273K$

Volume inside the gas cylinder: $TankVolume := 69.9L$

Pressure readings on the cylinder at the start and end of the test (steady-state):

$$P_{start} := 105 \frac{kgf}{cm^2} = 1493\,psi \qquad P_{end} := 90 \frac{kgf}{cm^2} = 1280\,psi$$

Mass of nitrogen inside the cylinder at the start and end of the test (steady-state):

$$m_{start} := \frac{P_{start} \cdot TankVolume}{R_{Nitrogen} \cdot T} = 8.394\,kg \qquad m_{end} := \frac{P_{end} \cdot TankVolume}{R_{Nitrogen} \cdot T} = 7.195\,kg$$

$$\Delta m := m_{start} - m_{end} = 1.199\,kg$$

Change in mass during the test (steady-state):

The pressure readings were taken at 8:51:10 AM and 8:54:15 AM, from a standard wall clock. The test duration is calculated below:

$$T_{start} := 51 \cdot 60s + 10s = 3070\,s \qquad T_{end} := 54 \cdot 60s + 15s = 3255\,s$$

$$\Delta t := T_{end} - T_{start} = 185\,s$$

The test (steady-state) lasted 185 seconds.

Divide the change in mass by the change in time during the steady-state interval to get a time-averaged mass-flow value:

$$m' := \frac{\Delta m}{\Delta t} = 0.00648 \frac{kg}{s}$$

Common to direct flow-measurement systems is volumetric flow rate. Find the volumetric flow rate at one atmosphere, 0 degrees Celsius:

$$\rho = \frac{P}{RT} \qquad \rho := \frac{101kPa}{R_{Nitrogen} \cdot T} = 1.178 \frac{kg}{m^3} \qquad Vol' := \frac{m'}{\rho} = 330.177 \frac{L}{min}$$

Appendix B: Data

B.1: Raw data

B.2: Mass flow rate summary tables

B.3: Mass flow rates through the nozzle

B.4 Theoretical mass flow rates (Egli relations)

B.5 Graphical Results

B.1: Raw Data

N 8
Concentricity : non-concentric

Ph (psig)	Th (C)	Pl (psig)	Tl (C)
10	21	1.5	21
15	21	2.75	21
20	22	4.5	21
25	21	5.75	21
30	21	8	21
35	21	9.75	21
40	21	12	21

N 8
Concentricity : concentric

Ph (psig)	Th (C)	Pl (psig)	Tl (C)
10	22	1.5	21
15	21	2.5	21
20	22	4	21
25	21	6	21
30	21	7.5	21
35	21	9.75	21
40	21	12	21

N 7
Concentricity : non-concentric

Ph (psig)	Th (C)	Pl (psig)	Tl (C)
10	22	1.5	22
15	22	3.25	21
20	21	5	21
25	21	7	21
30	21	9	21
35	21	1.5	21
40	21	14	21

N 7

Concentricity : concentric

Ph (psig)	Th (C)	Pl (psig)	Tl (C)
10	22	1.5	21
15	21	3	21
20	21	4.75	21
25	21	6.5	21
30	21	8.5	21
35	21	11.25	21
40	21	13.5	21

N 6

Concentricity : non-concentric

Ph (psig)	Th (C)	Pl (psig)	Tl (C)
10	21	2	21
15	21	3.75	21
20	21	5.75	21
25	21	8	21
30	21	11.25	21
35	21	13	21
40	21	NA	21

N 6

Concentricity : concentric

Ph (psig)	Th (C)	Pl (psig)	Tl (C)
10	21	1.5	21
15	21	3.5	21
20	21	5.25	21
25	21	7.5	21
30	21	9.75	21
35	21	12.25	21
40	21	NA	21

N 5

Concentricity : non-concentric

Ph (psig)	Th (C)	Pl (psig)	Tl (C)
10	21	2	21
15	21	4.25	21
20	21	6.25	21
25	21	8.5	21
30	21	11	21
35	21	14	21
40	21	NA	21

N 5

Concentricity : concentric

Ph (psig)	Th (C)	Pl (psig)	Tl (C)
10	21	2	21
15	21	4	21
20	21	6	21
25	21	8.25	21
30	21	10.75	21
35	21	13.5	21
40	21	NA	21

N 4

Concentricity : non-concentric

Ph (psig)	Th (C)	Pl (psig)	Tl (C)
10	21	2.5	21
15	21	4.5	21
20	21	7	21
25	21	9.5	21
30	21	12	21
35	21	NA	21
40	21	NA	21

N	4
Concentricity :	concentric

Ph (psig)	Th (C)	Pl (psig)	Tl (C)
10	21	2.25	21
15	21	4.5	21
20	21	6.75	21
25	21	9	21
30	21	11.75	21
35	21	NA	21
40	21	NA	21

B.2: Mass flow rate summaries

The following tables summarize the mass flow rates calculated for each condition and methodology. N refers to the tooth number at which the tests were conducted. Mass flow is in kg/s.

N=8						
Ph (MPa)	Mass flow Concentric	Mass flow Non Concentric	Mass flow Egli Concentric	Mass flow Egli Non Concentric	Mass flow R134a Concentric	Mass flow R134a Non-concentric
0.1703	0.007828153	0.007828153	0.000422659	0.000440729	0.036600825	0.032516735
0.2048	0.009947116	0.01039788	0.000549048	0.000524063	0.05651699	0.045960815
0.2393	0.012353664	0.013031396	0.000662724	0.000615581	0.080593487	0.063780469
0.2737	0.014818273	0.014542017	0.00076807	0.000679271	0.110597131	0.083333842
0.3082	0.016334993	0.016795073	0.000879917	0.000789894	0.124427383	0.095165234
0.3427	0.018264863	0.018264863	0.000982224	0.000931177	0.124791224	0.100795527
0.3772	0.019902828	0.019902828	0.001084725	0.001065874	0.125084854	0.104719221

N=7						
Ph (MPa)	Mass flow Concentric	Mass flow Non Concentric	Mass flow Egli Concentric	Mass flow Egli Non Concentric	Mass flow R134a Concentric	Mass flow R134a Non-concentric
0.1703	0.007828153	0.007828153	0.000432803	0.000432803	0.037479235	0.037479235
0.2048	0.010825586	0.01123297	0.000554084	0.000549871	0.057035334	0.056601687
0.2393	0.013352888	0.013663983	0.000667613	0.000663792	0.081188059	0.080723352
0.2737	0.015349122	0.015853779	0.000779596	0.000772439	0.112256862	0.11122634
0.3082	0.017322012	0.017659396	0.000886615	0.000881115	0.125374588	0.124596768
0.3427	0.019383407	0.019559263	0.00098622	0.000982789	0.125298971	0.124863085
0.3772	0.02087432	0.021180348	0.001091455	0.001084674	0.125860945	0.125079017

B.2: Mass flow rate summaries

N=6						
Ph (MPa)	Mass flow Concentric	Mass flow Non Concentric	Mass flow Egli Concentric	Mass flow Egli Non Concentric	Mass flow R134a Concentric	Mass flow R134a Non-concentric
0.1703	0.007828153	0.008961805	0.000439688	0.000429489	0.038075441	0.037192267
0.2048	0.011622261	0.011995308	0.000554239	0.00054976	0.057051369	0.056590269
0.2393	0.013965436	0.014542017	0.000670392	0.000662233	0.081525907	0.080533779
0.2737	0.016334993	0.016795073	0.000777196	0.000769398	0.111911296	0.110788419
0.3082	0.018264863	0.019383407	0.000884266	0.000860952	0.125042316	0.121745588
0.3427	0.02023611	0.020559749	0.000983976	0.000976441	0.125013821	0.124056562
0.3772	NA	NA	NA	NA	NA	NA

N=5						
Ph (MPa)	Mass flow Concentric	Mass flow Non Concentric	Mass flow Egli Concentric	Mass flow Egli Non Concentric	Mass flow R134a Concentric	Mass flow R134a Non-concentric
0.1703	0.008961805	0.008961805	0.000430144	0.000430144	0.037248995	0.037248995
0.2048	0.012353664	0.012698649	0.000546009	0.000541314	0.056204157	0.055720873
0.2393	0.014818273	0.015087164	0.000659036	0.000654745	0.08014495	0.079623166
0.2737	0.017017812	0.017235979	0.000766564	0.000762487	0.110380321	0.109793198
0.3082	0.019023071	0.019204711	0.00087029	0.000866308	0.123065996	0.122502992
0.3427	0.02087432	0.021180348	0.000970171	0.000962194	0.123259947	0.122246405
0.3772	NA	NA	NA	NA	NA	NA

B.2: Mass flow rate summaries

N=4						
Ph (MPa)	Mass flow Concentric	Mass flow Non Concentric	Mass flow Egli Concentric	Mass flow Egli Non Concentric	Mass flow R134a Concentric	Mass flow R134a Non-concentric
0.1703	0.009469879	0.009947116	0.000418998	0.000413602	0.036283792	0.035816517
0.2048	0.013031396	0.013031396	0.000529156	0.000529156	0.054469336	0.054469336
0.2393	0.015604541	0.015853779	0.000637053	0.000632566	0.077471638	0.076925994
0.2737	0.017659396	0.018066779	0.00074378	0.000735239	0.107099514	0.105869691
0.3082	0.019732373	0.019902828	0.000842283	0.000838109	0.119105678	0.118515381
0.3427	NA	NA	NA	NA	NA	NA
0.3772	NA	NA	NA	NA	NA	NA

B.3: Mass flow rates through the nozzle

The following tables contain the mass flow rates through the nozzle of the test rig, and the intermediate values of the calculations used to determine them.

Non-concentric Test			N=8					
Ph (psig)	Ph (Pa)	Pl (psig)	Pl (Pa)	Pr (l:e)	Mach LE	Ve (m/s)	mdot (kg/s)	error
10	170306.5	1.5	111699	1.1048368	0.380096138	131.3036042	0.007828153	6.61065E-07
15	204781.5	2.75	120317.75	1.19008655	0.504869258	174.4062795	0.01039788	8.15172E-07
20	239256.5	4.5	132384	1.3094362	0.632739701	218.5789199	0.013031396	9.28516E-07
25	273731.5	5.75	141002.75	1.39468595	0.706087949	243.9169552	0.014542017	9.72817E-07
30	308206.5	8	156516.5	1.54813551	0.815485119	281.7080331	0.016795073	1.01218E-06
35	342681.5	9.75	168582.75	1.66748516	0.886850804	306.3611952	0.018264863	1.02197E-06
40	377156.5	12	184096.5	1.82093472	0.96638221	333.8351922	0.019902828	1.01977E-06
							average	9.18784E-07

Concentric Test			N=8					
Ph (psig)	Ph (Pa)	Pl (psig)	Pl (Pa)	Pr (l:e)	Mach LE	Ve (m/s)	mdot (kg/s)	error
10	170306.5	1.5	111699	1.1048368	0.380096138	131.3036042	0.007828153	6.61065E-07
15	204781.5	2.5	118594	1.1730366	0.4829824	166.8454993	0.009947116	7.91168E-07
20	239256.5	4	128936.5	1.2753363	0.599832403	207.2111464	0.012353664	9.03762E-07
25	273731.5	6	142726.5	1.41173591	0.71950157	248.5506692	0.014818273	9.79326E-07
30	308206.5	7.5	153069	1.51403561	0.793145943	273.9910004	0.016334993	1.00662E-06
35	342681.5	9.75	168582.75	1.66748516	0.886850804	306.3611952	0.018264863	1.02197E-06
40	377156.5	12	184096.5	1.82093472	0.96638221	333.8351922	0.019902828	1.01977E-06
							average	9.11955E-07

Non-concentric Test			N=7					
Ph (psig)	Ph (Pa)	Pl (psig)	Pl (Pa)	Pr (l:e)	Mach LE	Ve (m/s)	mdot (kg/s)	error
10	170306.5	1.5	111699	1.1048368	0.380096138	131.3036042	0.007828153	6.61065E-07
15	204781.5	3.25	123765.25	1.22418645	0.545417089	188.413463	0.01123297	8.56111E-07
20	239256.5	5	135831.5	1.3435361	0.663454995	229.1894694	0.013663983	9.48879E-07
25	273731.5	7	149621.5	1.47993571	0.769780579	265.9194725	0.015853779	9.99477E-07
30	308206.5	9	163411.5	1.61633531	0.857452324	296.2055371	0.017659396	1.01936E-06
35	342681.5	11.5	180649	1.78683482	0.949700426	328.0724967	0.019559263	1.02129E-06
40	377156.5	14	197886.5	1.95733432	1.028412222	355.2633609	0.021180348	1.0096E-06
							average	9.30827E-07

B.3: Mass flow rates through the nozzle

Concentric Test			N=7					
Ph (psig)	Ph (Pa)	Pl (psig)	Pl (Pa)	Pr (l:e)	Mach LE	Ve (m/s)	mdot (kg/s)	error
10	170306.5	1.5	111699	1.1048368	0.380096138	131.3036042	0.007828153	6.61065E-07
15	204781.5	3	122041.5	1.2071365	0.525636567	181.5803133	0.010825586	8.36716E-07
20	239256.5	4.75	134107.75	1.32648615	0.648349762	223.9713907	0.013352888	9.39194E-07
25	273731.5	6.5	146174	1.44583581	0.745276941	257.45473	0.015349122	9.90484E-07
30	308206.5	8.6	160653.5	1.58905539	0.841070663	290.5465185	0.017322012	1.01705E-06
35	342681.5	11.25	178925.25	1.76978487	0.941161751	325.1228249	0.019383407	1.02186E-06
40	377156.5	13.5	194439	1.92323442	1.013553021	350.1302737	0.02087432	1.01266E-06
							average	9.25576E-07

Non-concentric Test			N=6					
Ph (psig)	Ph (Pa)	Pl (psig)	Pl (Pa)	Pr (l:e)	Mach LE	Ve (m/s)	mdot (kg/s)	error
10	170306.5	2	115146.5	1.1389367	0.435140636	150.3186384	0.008961805	7.3414E-07
15	204781.5	3.75	127212.75	1.25828635	0.582432427	201.2003523	0.011995308	8.89436E-07
20	239256.5	5.75	141002.75	1.39468595	0.706087949	243.9169552	0.014542017	9.72817E-07
25	273731.5	8	156516.5	1.54813551	0.815485119	281.7080331	0.016795073	1.01218E-06
30	308206.5	11.25	178925.25	1.76978487	0.941161751	325.1228249	0.019383407	1.02186E-06
35	342681.5	13	190991.5	1.88913452	0.998279026	344.8538966	0.020559749	1.0154E-06
40	377156.5	NA						
							average	9.40972E-07

Concentric Test			N=6					
Ph (psig)	Ph (Pa)	Pl (psig)	Pl (Pa)	Pr (l:e)	Mach LE	Ve (m/s)	mdot (kg/s)	error
10	170306.5	1.5	111699	1.1048368	0.380096138	131.3036042	0.007828153	6.61065E-07
15	204781.5	3.5	125489	1.2412364	0.564319123	194.9431406	0.011622261	8.73613E-07
20	239256.5	5.25	137555.25	1.36058605	0.678092057	234.245819	0.013965436	9.5766E-07
25	273731.5	7.5	153069	1.51403561	0.793145943	273.9910004	0.016334993	1.00662E-06
30	308206.5	9.75	168582.75	1.66748516	0.886850804	306.3611952	0.018264863	1.02197E-06
35	342681.5	12.5	187544	1.85503462	0.982564763	339.4254295	0.02023611	1.01779E-06
40	377156.5	NA						
							average	9.2312E-07

B.3: Mass flow rates through the nozzle

Non-concentric Test			N=5					
Ph (psig)	Ph (Pa)	Pl (psig)	Pl (Pa)	Pr (l:e)	Mach LE	Ve (m/s)	mdot (kg/s)	error
10	170306.5	2	115146.5	1.1389367	0.435140636	150.3186384	0.008961805	7.3414E-07
15	204781.5	4.25	130660.25	1.29238625	0.616583147	212.9976642	0.012698649	9.16744E-07
20	239256.5	6.25	144450.25	1.42878586	0.732557554	253.060838	0.015087164	9.85198E-07
25	273731.5	8.5	159964	1.58223541	0.836893336	289.1034675	0.017235979	1.01636E-06
30	308206.5	11	177201.5	1.75273492	0.932485117	322.1254957	0.019204711	1.02229E-06
35	342681.5	14	197886.5	1.95733432	1.028412222	355.2633609	0.021180348	1.0096E-06
40	377156.5	NA						
							average	9.4739E-07

Concentric Test			N=5					
Ph (psig)	Ph (Pa)	Pl (psig)	Pl (Pa)	Pr (l:e)	Mach LE	Ve (m/s)	mdot (kg/s)	error
10	170306.5	2	115146.5	1.1389367	0.435140636	150.3186384	0.008961805	7.3414E-07
15	204781.5	4	128936.5	1.2753363	0.599832403	207.2111464	0.012353664	9.03762E-07
20	239256.5	6	142726.5	1.41173591	0.71950157	248.5506692	0.014818273	9.79326E-07
25	273731.5	8.25	158240.25	1.56518546	0.826300206	285.4440876	0.017017812	1.01443E-06
30	308206.5	10.75	175477.75	1.73568497	0.923665628	319.0788174	0.019023071	1.02257E-06
35	342681.5	13.5	194439	1.92323442	1.013553021	350.1302737	0.02087432	1.01266E-06
40	377156.5	NA						
							average	9.44481E-07

Non-concentric Test			N=4					
Ph (psig)	Ph (Pa)	Pl (psig)	Pl (Pa)	Pr (l:e)	Mach LE	Ve (m/s)	mdot (kg/s)	error
10	170306.5	2.5	118594	1.1730366	0.4829824	166.8454993	0.009947116	7.91168E-07
15	204781.5	4.5	132384	1.3094362	0.632739701	218.5789199	0.013031396	9.28516E-07
20	239256.5	7	149621.5	1.47993571	0.769780579	265.9194725	0.015853779	9.99477E-07
25	273731.5	9.5	166859	1.65043521	0.877232853	303.0386893	0.018066779	1.02133E-06
30	308206.5	12	184096.5	1.82093472	0.96638221	333.8351922	0.019902828	1.01977E-06
35	342681.5	NA						
40	377156.5	NA						
							average	9.52053E-07

B.3: Mass flow rates through the nozzle

Concentric Test			N=4	With Nozzle				
Ph (psig)	Ph (Pa)	Pl (psig)	Pl (Pa)	Pr (l:e)	Mach LE	Ve (m/s)	mdot (kg/s)	error
10	170306.5	2.25	116870.25	1.15598665	0.459810156	158.8406845	0.009469879	7.64319E-07
15	204781.5	4.5	132384	1.3094362	0.632739701	218.5789199	0.013031396	9.28516E-07
20	239256.5	6.75	147897.75	1.46288576	0.757678821	261.7389398	0.015604541	9.9523E-07
25	273731.5	9	163411.5	1.61633531	0.857452324	296.2055371	0.017659396	1.01936E-06
30	308206.5	11.75	182372.75	1.80388477	0.958105781	330.9761131	0.019732373	1.0206E-06
35	342681.5	NA		0				
40	377156.5	NA						
							average	9.45604E-07

B.4: Egli Relations Mass Flow Rate Analysis

The following tables contain the mass flow rates determined through the Egli relations, and the intermediate values of the calculations required to reach mass flow rate.

8 Teeth		Non-concentric							
PH (Pa)	PL (Pa)	Pr	N (teeth)	Cr	Ct	X1	X2	Cc	mdot (kg/s)
170306.5	104804	0.61538462	8	0.8519906	0.28762999	14.7006792	1.2324	2.51687693	0.000440729
204781.5	128936.5	0.62962963	8	0.8519906	0.28362694	14.7006792	1.2324	2.51687693	0.000524063
239256.5	149621.5	0.62536023	8	0.8519906	0.28484291	14.7006792	1.2324	2.51687693	0.000615581
273731.5	180649	0.65994962	8	0.8519906	0.27457631	14.7006792	1.2324	2.51687693	0.000679271
308206.5	194439	0.63087248	8	0.8519906	0.28327032	14.7006792	1.2324	2.51687693	0.000789894
342681.5	194439	0.56740443	8	0.8519906	0.30002954	14.7006792	1.2324	2.51687693	0.000931177
377156.5	194439	0.51553931	8	0.8519906	0.31170887	14.7006792	1.2324	2.51687693	0.001065874

8 Teeth		Concentric							
PH (Pa)	PL (Pa)	Pr	N (teeth)	Cr	Ct	X1	X2	Cc	mdot (kg/s)
170306.5	111699	0.65587045	8	0.8519906	0.27583754	14.7006792	1.2324	2.51687693	0.000422659
204781.5	118594	0.57912458	8	0.8519906	0.29714884	14.7006792	1.2324	2.51687693	0.000549048
239256.5	128936.5	0.5389049	8	0.8519906	0.30665701	14.7006792	1.2324	2.51687693	0.000662724
273731.5	142726.5	0.52141058	8	0.8519906	0.31047081	14.7006792	1.2324	2.51687693	0.00076807
308206.5	153069	0.4966443	8	0.8519906	0.31555421	14.7006792	1.2324	2.51687693	0.000879917
342681.5	168582.75	0.49195171	8	0.8519906	0.31647693	14.7006792	1.2324	2.51687693	0.000982224
377156.5	184096.5	0.488117	8	0.8519906	0.31722159	14.7006792	1.2324	2.51687693	0.001084725

7 Teeth		Non-concentric							
PH (Pa)	PL (Pa)	Pr	N (teeth)	Cr	Ct	X1	X2	Cc	mdot (kg/s)
170306.5	111699	0.65587045	7	0.8519906	0.29664278	14.4370066	1.2106	2.39652189	0.000432803
204781.5	123765.25	0.6043771	7	0.8519906	0.31253954	14.4370066	1.2106	2.39652189	0.000549871
239256.5	135831.5	0.56772334	7	0.8519906	0.3225765	14.4370066	1.2106	2.39652189	0.000663792
273731.5	149621.5	0.5465995	7	0.8519906	0.32791791	14.4370066	1.2106	2.39652189	0.000772439
308206.5	163411.5	0.53020134	7	0.8519906	0.33185271	14.4370066	1.2106	2.39652189	0.000881115
342681.5	180649	0.52716298	7	0.8519906	0.33256202	14.4370066	1.2106	2.39652189	0.000982789
377156.5	197886.5	0.52468007	7	0.8519906	0.33313714	14.4370066	1.2106	2.39652189	0.001084674

B.4: Egli Relations Mass Flow Rate Analysis

6 Teeth		Non-concentric							
PH (Pa)	PL (Pa)	Pr	N (teeth)	Cr	Ct	X1	X2	Cc	mdot (kg/s)
170306.5	115146.5	0.67611336	6	0.8519906	0.31452074	13.9992301	1.1888	2.24299257	0.000429489
204781.5	127212.75	0.62121212	6	0.8519906	0.33386501	13.9992301	1.1888	2.24299257	0.00054976
239256.5	141002.75	0.58933718	6	0.8519906	0.34384695	13.9992301	1.1888	2.24299257	0.000662233
273731.5	156516.5	0.57178841	6	0.8519906	0.34898392	13.9992301	1.1888	2.24299257	0.000769398
308206.5	178925.25	0.58053691	6	0.8519906	0.34645384	13.9992301	1.1888	2.24299257	0.000860952
342681.5	190991.5	0.55734406	6	0.8519906	0.35303023	13.9992301	1.1888	2.24299257	0.000976441
377156.5	0	0	6	0.8519906	0.41858674	13.9992301	1.1888	2.24299257	0.001275581

6 Teeth		Concentric							
PH (Pa)	PL (Pa)	Pr	N (teeth)	Cr	Ct	X1	X2	Cc	mdot (kg/s)
170306.5	111699	0.65587045	6	0.8519906	0.3219894	13.9992301	1.1888	2.24299257	0.000439688
204781.5	125489	0.61279461	6	0.8519906	0.33658536	13.9992301	1.1888	2.24299257	0.000554239
239256.5	137555.25	0.57492795	6	0.8519906	0.34808294	13.9992301	1.1888	2.24299257	0.000670392
273731.5	153069	0.55919395	6	0.8519906	0.35252099	13.9992301	1.1888	2.24299257	0.000777196
308206.5	168582.75	0.54697987	6	0.8519906	0.35583541	13.9992301	1.1888	2.24299257	0.000884266
342681.5	187544	0.5472837	6	0.8519906	0.35575432	13.9992301	1.1888	2.24299257	0.000983976
377156.5	0	0	6	0.8519906	0.41858674	13.9992301	1.1888	2.24299257	0.001275581

5 Teeth		Non-concentric							
PH (Pa)	PL (Pa)	Pr	N (teeth)	Cr	Ct	X1	X2	Cc	mdot (kg/s)
170306.5	115146.5	0.67611336	5	0.8519906	0.34540922	13.2723887	1.167	2.04552643	0.000430144
204781.5	130660.25	0.63804714	5	0.8519906	0.36047056	13.2723887	1.167	2.04552643	0.000541314
239256.5	144450.25	0.6037464	5	0.8519906	0.37277714	13.2723887	1.167	2.04552643	0.000654745
273731.5	159964	0.58438287	5	0.8519906	0.37923571	13.2723887	1.167	2.04552643	0.000762487
308206.5	177201.5	0.57494407	5	0.8519906	0.3822624	13.2723887	1.167	2.04552643	0.000866308
342681.5	197886.5	0.57746479	5	0.8519906	0.38146174	13.2723887	1.167	2.04552643	0.000962194
377156.5	0	0	5	0.8519906	0.45969535	13.2723887	1.167	2.04552643	0.001277527

B.4: Egli Relations Mass Flow Rate Analysis

5 Teeth		Concentric							
PH (Pa)	PL (Pa)	Pr	N (teeth)	Cr	Ct	X1	X2	Cc	mdot (kg/s)
170306.5	115146.5	0.67611336	5	0.8519906	0.34540922	13.2723887	1.167	2.04552643	0.000430144
204781.5	128936.5	0.62962963	5	0.8519906	0.36359703	13.2723887	1.167	2.04552643	0.000546009
239256.5	142726.5	0.59654179	5	0.8519906	0.37522002	13.2723887	1.167	2.04552643	0.000659036
273731.5	158240.25	0.57808564	5	0.8519906	0.38126369	13.2723887	1.167	2.04552643	0.000766564
308206.5	175477.75	0.56935123	5	0.8519906	0.38401922	13.2723887	1.167	2.04552643	0.00087029
342681.5	194439	0.56740443	5	0.8519906	0.38462443	13.2723887	1.167	2.04552643	0.000970171
377156.5	0	0	5	0.8519906	0.45969535	13.2723887	1.167	2.04552643	0.001277527

4 Teeth		Non-concentric							
PH (Pa)	PL (Pa)	Pr	N (teeth)	Cr	Ct	X1	X2	Cc	mdot (kg/s)
170306.5	118594	0.69635628	4	0.8519906	0.37883209	12.0656118	1.1452	1.7933335	0.000413602
204781.5	132384	0.64646465	4	0.8519906	0.40192777	12.0656118	1.1452	1.7933335	0.000529156
239256.5	149621.5	0.62536023	4	0.8519906	0.41079674	12.0656118	1.1452	1.7933335	0.000632566
273731.5	166859	0.60957179	4	0.8519906	0.41710892	12.0656118	1.1452	1.7933335	0.000735239
308206.5	184096.5	0.59731544	4	0.8519906	0.42182629	12.0656118	1.1452	1.7933335	0.000838109
342681.5	0	0	4	0.8519906	0.51715275	12.0656118	1.1452	1.7933335	0.001143632
377156.5	0	0	4	0.8519906	0.51715275	12.0656118	1.1452	1.7933335	0.001260012

4 Teeth		Concentric							
PH (Pa)	PL (Pa)	Pr	N (teeth)	Cr	Ct	X1	X2	Cc	mdot (kg/s)
170306.5	116870.25	0.68623482	4	0.8519906	0.38377447	12.0656118	1.1452	1.7933335	0.000418998
204781.5	132384	0.64646465	4	0.8519906	0.40192777	12.0656118	1.1452	1.7933335	0.000529156
239256.5	147897.75	0.61815562	4	0.8519906	0.41371056	12.0656118	1.1452	1.7933335	0.000637053
273731.5	163411.5	0.59697733	4	0.8519906	0.42195421	12.0656118	1.1452	1.7933335	0.00074378
308206.5	182372.75	0.5917226	4	0.8519906	0.42392731	12.0656118	1.1452	1.7933335	0.000842283
342681.5	0	0	4	0.8519906	0.51715275	12.0656118	1.1452	1.7933335	0.001143632
377156.5	0	0	4	0.8519906	0.51715275	12.0656118	1.1452	1.7933335	0.001260012

B.5 Graphical Results

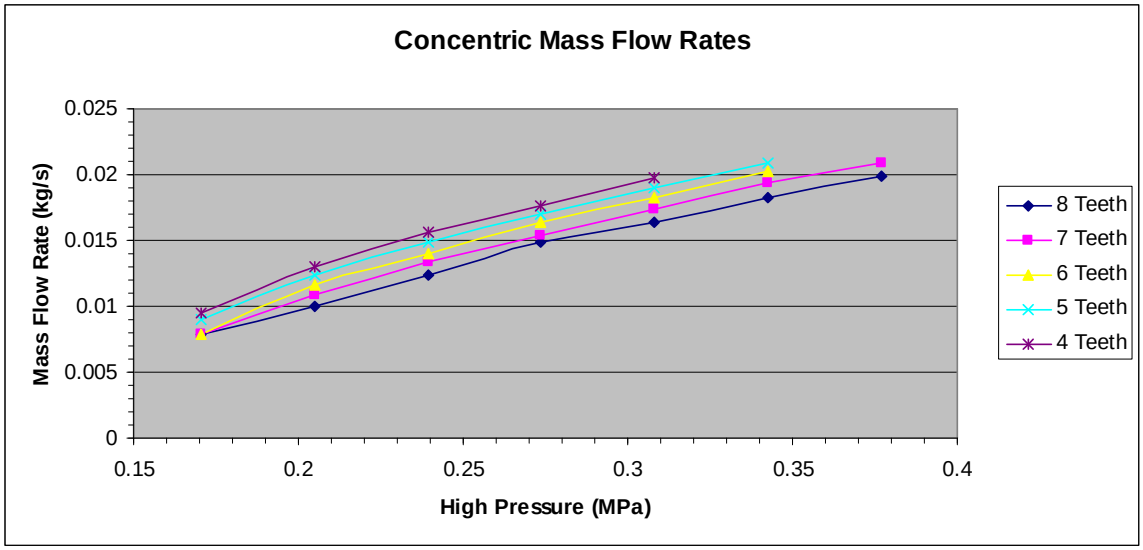

Figure B1: Plots all of the data taken during concentric testing. The mass flow rate is plotted as a function of pressure.

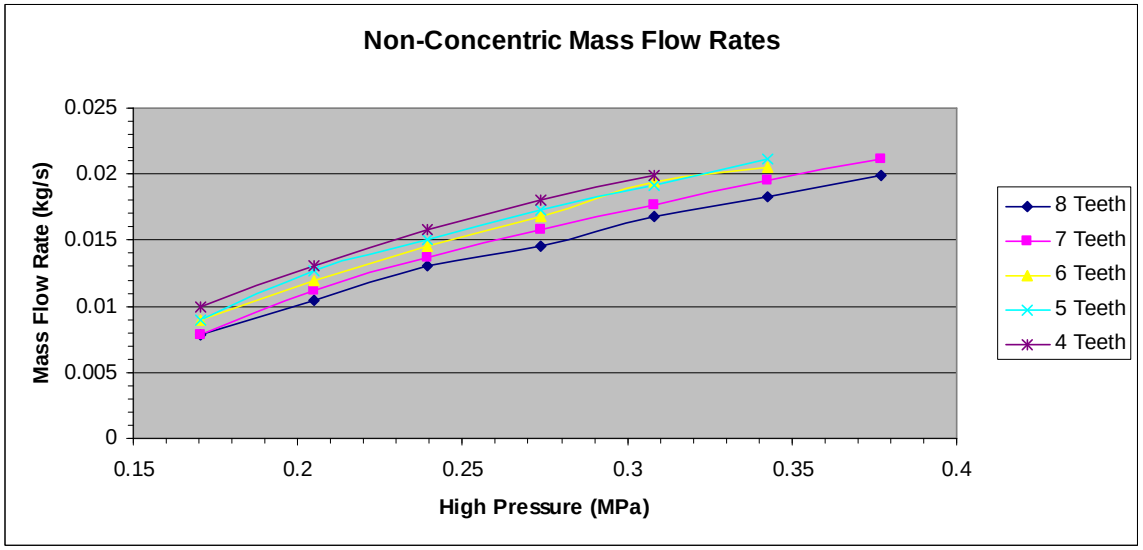

Figure B2: Plots all of the data taken during non-concentric testing. The mass flow rate is plotted as a function of pressure.

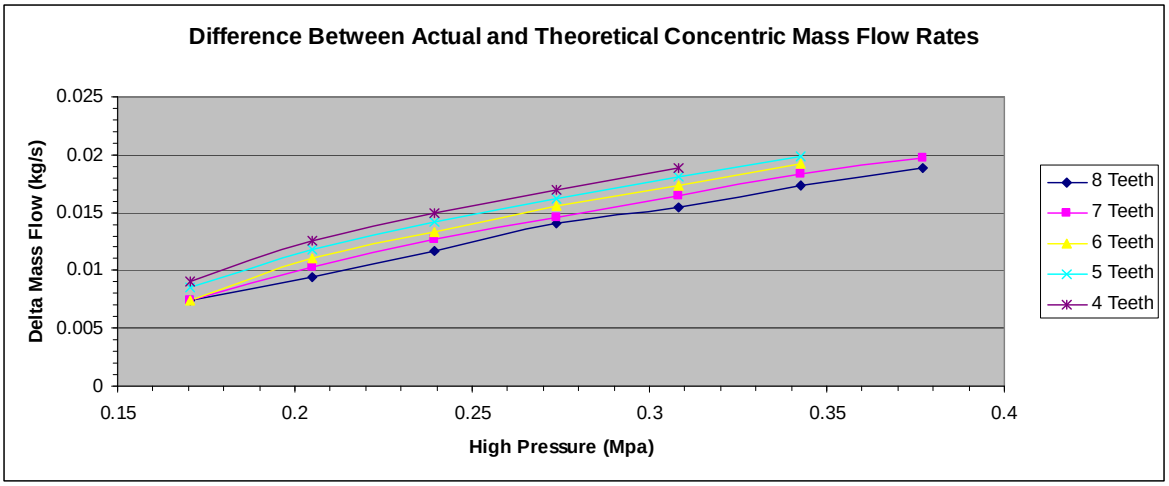

Figure B3: graphs the difference in flow mates between the Mach number relations and the Egli relations for each tooth test. To find delta mass flow rate the Egli flow was subtracted from the Mach flow.

The following five graphs compare the mass flow rates of Non-concentric to Concentric flow for each of the tooth numbers tested.

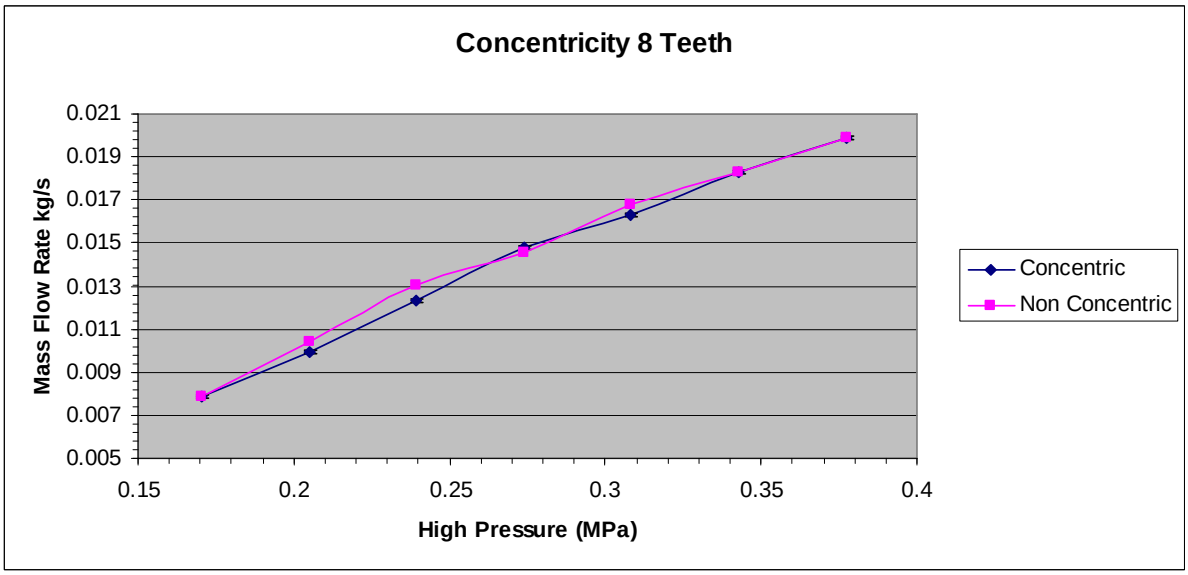

Figure B4

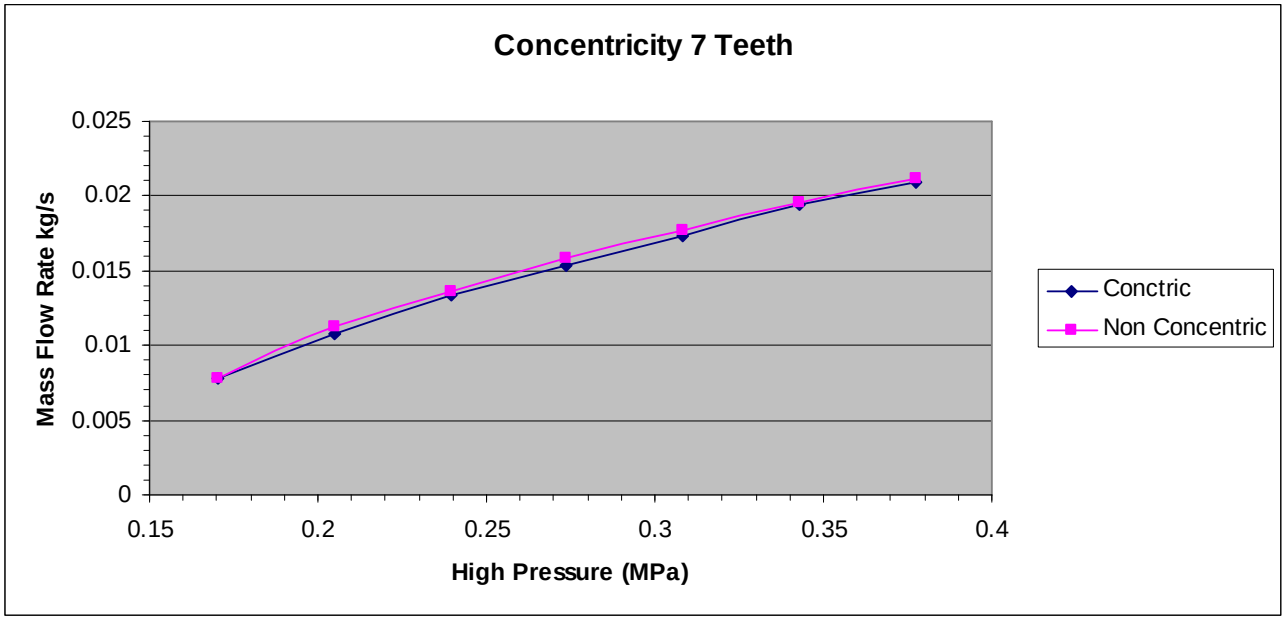

Figure B5

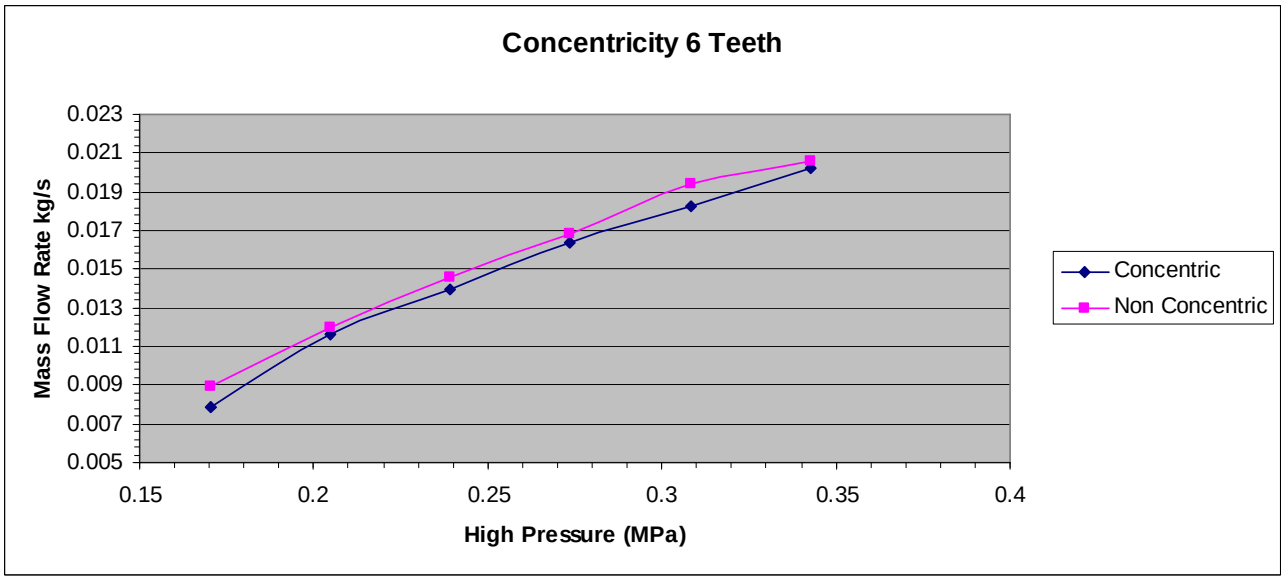

Figure B6

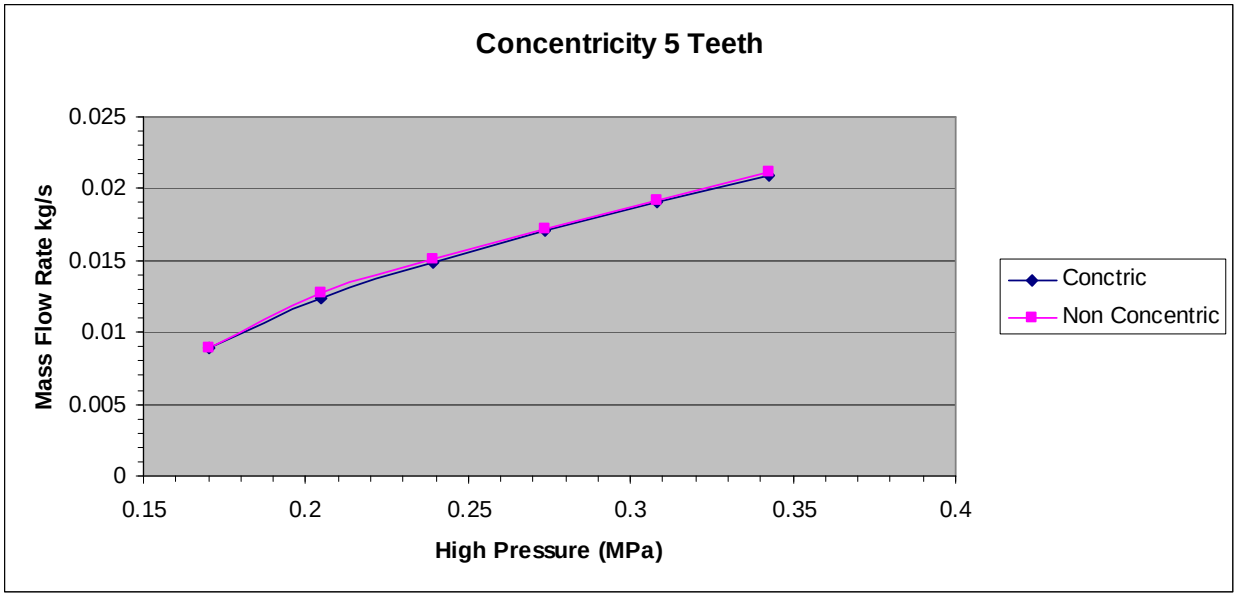

Figure B7

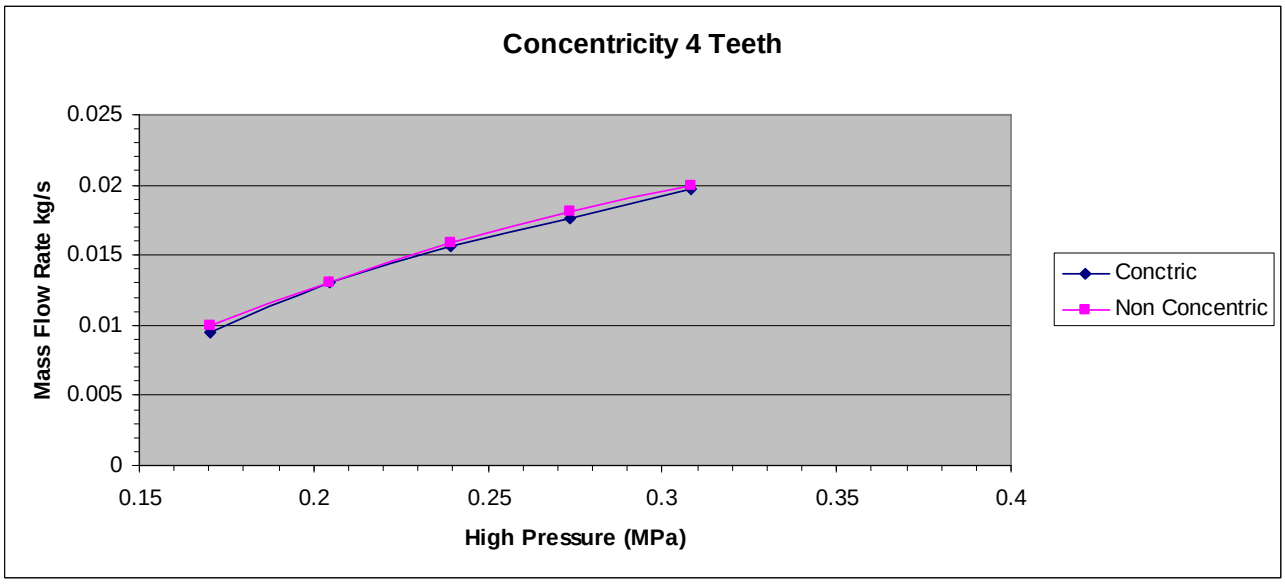

Figure B8

Appendix C: Detail Design Drawings